Journal of Advanced Research xxx (xxxx) xxx

Contents lists available at ScienceDirect

Journal of Advanced Research

journal homepage: www.elsevier.com/locate/jare

Original Manuscript

Genotype-driven variations in lncRNA expression underlie predisposition to high-grade serous ovarian cancer

Mingming Lu [a,b,c,d,e,f,1], Yanan Chu [d,e,1], Ziwei Zhu [a,b,1], Hong Zhou [a,b,1], Danfei Zhu [a,b,1], Siyi Chen [a,b], Congfan Bu [c,d,e,f], Qiheng Qian [c,d,e,f], Chen Gao [j], Meiye Jiang [c,d,e,f], Hao Zhang [c,d,e,f], Jinyue Wang [c,d,e,f], Jingyao Zeng [c,d,e], Zhewen Zhang [c,d,e], Qiong Zhao [a,b], Shuai Liu [b], Xudong Fu [b], Na Kong [b], Francis KM Chan [b], Yongcheng Wang [b,i], Guangyi Jiang [g,h,*], Yu Kang [d,e,f,**], Xin Sheng [a,b,***]

[a] Department of Nephrology, Children's Hospital, Zhejiang University School of Medicine, National Clinical Research Center for Children and Adolescents' Health and Diseases, Hangzhou, Zhejiang 310052, China
[b] Liangzhu Laboratory, Zhejiang University, 1369 West Wenyi Road, Hangzhou, Zhejiang 311121, China
[c] National Genomics Data Center, China National Center for Bioinformation, Beijing 100101, China
[d] China National Center for Bioinformation, Beijing 100101, China
[e] Beijing Institute of Genomics, Chinese Academy of Sciences, Beijing 100101, China
[f] University of Chinese Academy of Sciences, Beijing 100049, China
[g] Zhejiang Cancer Hospital, Hangzhou, Zhejiang 310022, China
[h] Hangzhou Institute of Medicine (HIM), Chinese Academy of Sciences, Hangzhou, Zhejiang 310022, China
[i] Department of Laboratory Medicine of The First Affiliated Hospital, Zhejiang University School of Medicine, Hangzhou, Zhejiang 310000, China
[j] HaiDe College, Ocean University of China, Qingdao 266003, China

HIGHLIGHTS

- lncRNAs contribute to a greater proportion to HGSOC heritability than PCGs.
- We mapped lnc-eQTLs and PCG-eQTLs in HGSOC tumors.
- We prioritized causal genes in HGSOC tumors and whole blood.
- We characterized a single-cell full-length transcriptome atlas in HGSOC tumors.
- We validated the role of *CRHR1-IT1* in promoting apoptosis and inhibiting the growth of HGSOC cells.

GRAPHICAL ABSTRACT

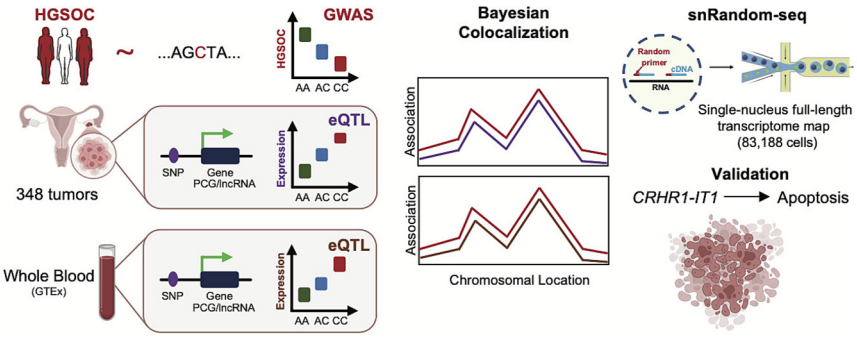

ARTICLE INFO

Article history:
Received 26 June 2025
Revised 29 November 2025
Accepted 3 January 2026
Available online xxxx

ABSTRACT

Introduction: New effective early diagnosis strategies and therapeutic targets are desperately needed for high-grade serous ovarian cancer (HGSOC). Previous functional interpretation of HGSOC genome-wide association studies (GWAS) have largely overlooked the role of long non-coding RNAs (lncRNAs).
Objectives: Our study aims to identify novel causal genes, particularly lncRNAs, that contribute to HGSOC susceptibility and to explore whether their may provide preliminary insights relevant to early detection or therapeutic development.

* Corresponding author at: Zhejiang Cancer Hospital, Hangzhou, Zhejiang 310022, China.
** Corresponding author at: China National Center for Bioinformation, Beijing 100101, China.
*** Corresponding author at: Department of Nephrology, Children's Hospital, Zhejiang University School of Medicine, National Clinical Research Center for Children and Adolescents' Health and Diseases, Hangzhou, Zhejiang 310052, China.
E-mail addresses: jianggy@zjcc.org.cn (G. Jiang), kangy@big.ac.cn (Y. Kang), shengxin@zju.edu.cn (X. Sheng).
[1] These authors contributed equally.

https://doi.org/10.1016/j.jare.2026.01.014
2090-1232/© 2026 The Author(s). Published by Elsevier B.V. on behalf of Cairo University.
This is an open access article under the CC BY-NC-ND license (http://creativecommons.org/licenses/by-nc-nd/4.0/).

Please cite this article as: M. Lu, Y. Chu, Z. Zhu et al., Genotype-driven variations in lncRNA expression underlie predisposition to high-grade serous ovarian cancer, Journal of Advanced Research, https://doi.org/10.1016/j.jare.2026.01.014

Keywords:
eQTL
Colocalization
lncRNA
post-GWAS
CRHR1-IT1
Ovarian cancer

Methods: We mapped genotype effects on the expression of both protein-coding genes (PCGs) and lncRNAs in 348 HGSOC tumor samples. By performing Bayesian colocalization analysis, we prioritized causal genes in HGSOC tumors and whole blood, respectively. Next, we generated a single-nucleus full-length transcriptome map of HGSOC tumor using snRandom-seq. Furthermore, we conducted *in vitro* assays to validate the functional role of lncRNA *CRHR1-IT1* in HGSOC.
Results: Our findings reveal that genetic variants significantly drive expression changes in both PCGs and lncRNAs. Notably, lncRNAs contribute a greater proportion of HGSOC heritability than PCGs. Using Bayesian colocalization analysis, we prioritized 22 high-fidelity causal genes in HGSOC tumors and whole blood, including *ARL17A* and *CRHR1-IT1*. Through snRandom-seq, we characterized the single-cell expression patterns of candidate susceptibility PCGs and lncRNAs in HGSOC tumors. Furthermore, we showed that elevated *CRHR1-IT1* expression promotes apoptosis and inhibits the growth of HGSOC cells *in vitro*.
Conclusion: Our study highlights the significant regulatory role of genetic variants on both protein-coding genes and lncRNAs in HGSOC. While these findings enhance our understanding of HGSOC susceptibility and may inform future efforts toward biomarker discovery or immune-related therapeutic exploration.
© 2026 The Author(s). Published by Elsevier B.V. on behalf of Cairo University. This is an open access article under the CC BY-NC-ND license (http://creativecommons.org/licenses/by-nc-nd/4.0/).

Introduction

Invasive epithelial ovarian cancer (EOC) is among the leading causes of gynecologic cancer in women worldwide, with greater than 314,000 new diagnoses and approximately 207,000 deaths each year [1]. Histological subtypes of invasive EOC vary in epidemiological [2–4] and genetic risk factors [5], clinical responses to platinum-based therapy [6,7], and cells of origin [8,9]. High-grade serous ovarian cancer (HGSOC) is the most prevalent histotype, accounting for 60–70 % of EOC cases and the majority of EOC mortality [10,11]. Current treatments mostly rely on traditional cytoreductive surgery combined with platinum-based chemotherapy, and the overall 5-year survival rate is still below 20 % for HGSOC due to the scarcity of effective early diagnosis strategies and the rapid development of chemoresistance [12–17]. Therefore, new oncogenes and tumor suppressors that could serve as effective diagnostic and therapeutic targets for HGSOC, are desperately needed. To prioritize the best targets, it is of critical importance to understand the germline genetic architecture of HGSOC, as previous studies consistently confirmed that genetically supported drug targets could substantially contribute to the successful development of new therapeutics [18,19].

HGSOC has a significant germline genetic component, with an estimated heritability around 20 to 40 % [15,17,20,21]. Known germline loss-of-function mutations in susceptibility genes, such as *BRCA1*, *BRCA2*, *TP53, BRIP1, MSH6,* and *RAD51C/D*, only account for about 10 % of cases [22–27]. The majority of genetic risk factors for HGSOC is due to common low-penetrance-susceptibility alleles [28]. Large-scale genome-wide association studies (GWASs) have so far identified 19 loci, where common single-nucleotide polymorphisms (SNPs) show statistically significant reproducible association with HGSOC predisposition [29–38], suggesting that germline genetic variants influence tumorigenesis. However, interpreting the likely biological mechanism of GWAS is challenging, as more than 90 % of risk variants lie in the non-protein-coding regions of the genome. Expression quantitative trait locus (eQTL) analysis has been a powerful approach to map risk variants to disease-causing genes [39–41]. By integrating of eQTL and GWAS, several previous studies have successfully prioritized putative susceptibility genes for HGSOC risk loci, such as *HOXD9* [42], *TERT* [42], *CHMP4C* [28], *ANKLE1/ABHD8* [29], and *GNL2* [43].

Although long non-coding RNAs (lncRNAs) dominate the transcriptome in human cells, most efforts to interpret the functional consequences of non-coding risk variants have primarily focused on their regulatory effects on protein-coding genes (PCGs), greatly neglecting lncRNAs, which have been increasingly shown to play critical roles in chemoresistance, tumorigenesis, tumor progression, and metastasis [29,44–51]. LncRNAs are likely to act as scaffolds, guides, or decoys to alter DNA-protein binding or protein–protein interactions [49,52], resulting in dysregulation in cell proliferation, differentiation and apoptosis [53,54]. Previous investigations of the correlation between disease-associated SNPs and lncRNA expression have successfully nominated several potential disease-causing lncRNAs, such as *PCAT1* in promoting prostate cancer cell growth [55] and *LINC01475* in influencing ulcerative colitis susceptibility [56]. Therefore, systematic interrogation of the regulation from germline variants on lncRNAs (lncRNA-eQTLs) could provide new insights into how risk variants contribute to HGSOC pathogenesis via non-coding genome and improve new therapeutic targets identification.

In this study, we generated a comprehensive atlas of eQTLs for both PCGs and lncRNAs, utilizing 348 HGSOC tumor samples with matched high-quality genotype and gene expression data from the Cancer Genome Atlas (TCGA) [57]. Our findings indicate that germline variants play crucial roles in modulating the expression of not only PCGs but also lncRNAs, which could further contribute to HGSOC predisposition. Using Bayesian colocalization analysis [58], we prioritized 10 susceptibility genes for HGSOC, comprising 6 PCGs and 4 lncRNAs, where genotype-driven gene expression changes are highly associated with HGSOC risk in high-grade ovarian tumors. Five of these genes, such as *ARL17A* and *CRHR1-IT1*, also showed an association with HGSOC predisposition in whole blood. We characterized the expression patterns of susceptibility PCGs and lncRNAs using single-nucleus resolution transcriptome maps of the human HGSOC tumor. In addition, we conducted *in vitro* assays and validated the functional role of *CRHR1-IT1* in promoting apoptosis of ovarian cancer cells. Our study may help inform future efforts toward early detection and the development of new therapeutic strategies for HGSOC.

Materials and methods

Genotype and RNA-seq data processing for eQTL analysis

We downloaded matched genotype and quantified gene expression data for 350 primary HGSOC tumor samples from the TCGA data portal (https://tcga-data.nci.nih.gov/tcga/) [57]. The TCGA germline variants data were genotyped using the Affymetrix Genome-Wide Human SNP Array 6.0. Quality control of raw genotype data was performed using PLINK (v2.0) [59] (https://www.cog-genomics.org/plink2/). We excluded samples with misgendering, contamination, or low call rates. SNPs on sex chromosomes, monomorphic SNPs, and those with a minor allele frequency (MAF) 1 %, Hardy–Weinberg equilibrium P-value <1.0E-06, or call rate <95 % were removed as well. In total, we excluded 2 contaminated samples with high PIHAT values (>0.2). This left 348 individ-

uals and 771,697 SNPs for further analysis (**Table S1**). To better understand the genetic background of the TCGA HGSOC samples, we performed Principal Components Analysis (PCA) on the genotype data of these 348 HGSOC subjects, along with 2,504 genotyped data from the 1,000 Genomes Project Phase 3 [60], using Genome-wide Complex Trait Analysis (GCTA) [61]. Most samples in our study clustered amongst the European populations, as shown in **Fig. S1**. The first 2 principal components (PCs) were used in the linear regression model for eQTL analysis.

To increase eQTL discovery power, autosomal variants were pre-phased by SHAPEIT2 [62] and subsequently imputed with IMPUTE2 [63], using 1,000 Genomes Project Phase 3 as the reference panel. Before imputation, indels and SNPs absent or incompatible with the 1,000 Genomes Project dataset were removed. Imputed SNPs with MAF <1 %, Hardy-Weinberg Equilibrium P-value <1E-06, and imputation confidence score INFO (a measure of r^2) <0.4 (estimated by SNPTEST [64] were further excluded. Consequently, 8,579,445 high-quality autosomal SNPs were used for eQTL analysis.

The TCGA level 3 RNA-seq data were aligned to the human genome based on GENCODE v22 annotations [65]. Next, we normalized the downloaded raw read counts across samples using the TMM method and then estimated gene expression levels as transcripts per million (TPM). Only genes with at least 0.1 TPM in more than two samples were identified as expressed and used for downstream eQTL analysis.

eQTL mapping

We performed *cis*-eQTL (further referred to as eQTL) mapping using 348 primary HGSOC samples for both protein-coding genes (PCGs) and lncRNAs (**Table S2**). Expression measurements for each PCG or lncRNA were quantile-normalized and then transformed into a rank-based standard normal expression using inverse normal-transformed (INT). To remove the effects of latent confounders, we estimated 40 and 60 PEER [66] factors on INT expression by adjusting for age, batch effect, and top 2 genotype PCs for PCG-eQTL and lncRNA-eQTL identification, respectively. We selected the number of PEER factors that maximized the detection of ePCGs and elncRNAs (**Fig. S2**), that is, PCGs and lncRNAs significantly associated with at least one SNP. eQTL mapping was then performed using the INT gene expression as the outcome and SNP dosage as the independent variable, adjusting for age, batch effect, top 2 genotype PCs, and the estimated PEER factors. Nominal P-values were calculated for all SNPs located within ±1 Mb of PCGs/lncRNAs using MatrixEQTL [67] with an additive linear regression mode. A permutation procedure was then implemented using FastQTL [68] with the setting "-permute 10000". We adopted Beta distribution-adjusted empirical P-values to calculate q using Storey's q method [69], and identified eGenes with a q cutoff $\leq$0.05. Next, we defined an empirical P threshold, P_t, as the empirical P of the PCG/lncRNA closest to the 0.05 FDR threshold. P_t was used to estimate the nominal P cutoff for each gene based on the Beta distribution model of the minimum P distribution f(P_{min}), generated from the permutations for the gene. SNPs having a lower nominal P than the gene-level cutoff were identified as eSNPs, i.e., SNPs that significantly regulated at least one PCG or lncRNA [40].

Differentially expressed genes identification

To minimize computational batch effects causing by different data analysis pipelines in TCGA and GTEx (v7; https://gtexportal.org/home/) [70] cohorts, we downloaded the recomputed gene expression data in the ovaries of the TCGA HGSOC patients and GTEx healthy samples using a consistent analysis protocol from UCSC Xena (https://xena.ucsc.edu/) [71]. The estimated gene expression was quantified as transcripts per kilobase million (TPM). Genes with TPM <0.1 in <5 % of samples were excluded from downstream analysis. Differentially expressed genes (DEGs) between HGSOC tumor and healthy samples were identified using a linear model combined with an empirical Bayes method in the R package limma [72]. This linear regression model adopted gene expression as the outcome and disease status as independent variable, adjusting for age. Genes with a Benjamini-Hochberg FDR <0.05 were identified as DEGs.

Colocalization analysis

To evaluate the posterior probabilities of inherited HGSOC risk and expression of both PCGs and lncRNAs sharing common genetic causal variants in a given region, we performed colocalization analysis on summary data of HGSOC GWAS [33] and eQTL data from HGSOC tumors and whole blood (from GTEx v7) [70] using coloc v5.2.3 [58]. We adopted the Phelan et al. HGSOC GWAS study based on 13,037 cases and 40,941 controls [33]. HGSOC associated variants with a P-value <5E-08 were selected. Accounting for the inflation caused by GWAS variants representing the same signal, we performed LD pruning using *swiss* (https://github.com/statgen/swiss) by discarding variants in LD $r^2 \geq$0.8 with the lead SNP at each locus. Genomic regions within ±100 kb of each pruned GWAS variant, that overlap with ePCGs or elncRNAs, were used in the coloc analysis. Posterior probability was then estimated using summary data of HGSOC GWAS and PCG-eQTLs/lncRNA-eQTLs to identify the colocalization regions. In the coloc results, H3 tests the hypothesis that both traits (e.g., HGSOC risk and gene expression) are associated but with independent causal variants, whereas H4 tests the hypothesis that both traits share the same causal variants (colocalization). In this study, coloc examines whether HGSOC risk and gene expression are associated and share the same causal variants (H4). We used PP4 (the posterior probability of H4) >0.8 as the threshold of colocalization, following our previous work and multiple high-impact colocalization studies that adopt the same posterior probability thresholds to ensure high-confidence signals [39–41,58,73]. Notably, PP4 is a Bayesian posterior probability rather than a frequentist P-value; therefore, multiple testing correction is not required, as coloc directly quantifies the probability of shared causal variants within each tested region under predefined priors. This approach is consistent with the methodological guildelines of coloc and with standard practice in the colocalization literature [58].

Sample procurement for snRandom-seq

Six high-grade tumor specimens used for single-nucleus Random-seq were obtained from the Biobank of Zhejiang Cancer Hospital (**Table S3**). One specimen was collected from the intestinal surface during primary debulking surgery, and one was obtained from adipose tissue during surgery for platinum-resistant recurrence. The remaining four specimens were collected from ovarian tissues during primary debulking surgery. All specimens were confirmed as high-grade tumors by pathologically review.

snRandom-seq-based FFPE single-nucleus transcriptome library construction and sequencing

We utilized the VITApilote High-Throughput Single-Cell Transcriptome Kit for FFPE samples (M20 Genomics, Cat# R20123124) for pre-library processing, library construction, and purification. The VITAcruizer Single-Cell Preparation System DP400 (M20 Genomics, Cat# E20000131) was employed for

single-cell partitioning, encapsulation, and nucleic acid capture. The experiments were carried out according to the manufacturer's instructions for the snRandom-seq workflow. The main workflow was as follows: FFPE samples were cut from paraffin block and washed twice with 1 mL Xylene (Aladdin, Cat# X112054) for 5 min at room temperature to remove the paraffin. The samples were then gently rehydrated by immersing them in a graded series of ethanol solutions (100 %, 90 %, 70 %, 50 %, and 30 %; Aladdin, Cat# E130059), starting with 100 % ethanol and ending with 30 % ethanol and subsequently transferred to water. The rehydrated tissue sections were permaeablized under mild conditions to maintain nuclear integrity, followed by *in situ* blocking of single-stranded DNA. Random primers were then added to initiate *in situ* reverse transcription of total nuclear RNA within the tissue section, generating cDNA fragments representative of the nuclear transcriptome. These cDNA fragments were subsequently ligated to universal sequencing adapters within the nuclei prior to nuclear isolation. The tissue section was then lysed into individual nuclei by gentle mechanical disruption and enzymatic digestion, and the resulting suspension was filtered through a 20 μm cell strainer (pluriSelect, Cat#43-10020-20). The reverse-transcribed single-nucleus suspension was mixed with reagents and barcoding beads containing 30-nt cell barcodes and 8-nt unique molecular identifiers (UMIs). This mixture was encapsuled, captured and barcoded using the VITAcruizer Single-Cell Preparation System DP400, resulting in barcoded cDNA strands. The barcoded cDNA was then extended, purified, and PCR-amplified to generate sequencing libraries containing P5 and P7 adapters. The libraries were sequenced on a Novaseq 6000 platform (Illumina) with 150 bp paired-end reads (**Table S3**).

Compared with conventional droplet-based sc/snRNA-seq platforms (e.g., 10x Genomics), snRandom-seq employes a random-primed reverse transcription strategy that captures a broader spectrum of nuclear transcripts, including non-polyadenylated RNAs. This feature makes it particularly suitable for profiling lncRNA expression from preserved or FFPE tumor tissues.

SnRandom-seq data processing

Primer sequences and adaptors were trimmed from the raw data. The UMI (8nts) and cell-specific barcode (30nts) for each Read1 were then extracted. Sequenced barcodes were merged if they could be uniquely assigned to the same accepted barcode with a Hamming distance of 2 nts or less. Sequencing reads were aligned to the human genome based on GENCODE v22 annotations [65] using the STARsolo module of the STAR aligner (version 2.7.10a) with appropriate parameters [74]. The expression data were further analyzed with Seurat (v5.0.2) [75]. For quality control, we excluded features expressed in fewer than 5 cells. Low-quality cells with fewer than 200 detected features or more than 5,000 features were also excluded. In addition, cells with more than 40 % mitochondrial transcripts were filtered out. Samples were integrated and batch effects were removed using the FindIntegrationAnchors function and the RunHarmony function [75–77]. PCA was performed and the first 35 Harmony-adjusted PCs were selected to generate a *k*-nearest neighbor graph with $k = 5$. Uniform manifold approximation and projection (UMAP) embeddings with a resolution of 0.8 were generated to visualize the data [78].

Human gynecologic tumor scRNA-seq data

We used the RNA-seq count matrix of 75,532 cells profiled from human gynecologic tumors of 11 patients (GSE173682) [79]. Data processing and normalization were performed using R package Seurat (v5.0.2) [75]. Features expressed in fewer than 5 cells were removed, and gene expression values were normalized with the default Seurat workflow. The top 3,000 highly variable genes were selected for downstream scaling. Cluster assignment of the cells was based on the annotations in Fig. S4 of the published dataset [79].

Cell culture and transfection experiment

The human ovarian adenocarcinoma cell line OVCAR3 (ATCC® HTB-161™) was purchased from ATCC (USA) and cultured in Roswell Park Memorial Institute 1640 Medium (RPMI-1640; Cat# 302001) supplemented with 20 % fetal bovine serum (Gibco, USA) and 0.01 mg/mL bovine insulin (Sigma, Cat# I6634). The human ovarian carcinoma cell line A2780 was a gift from Dr. Guangyi Jiang (Zhejiang Cancer Hospital) and cultured in the Dulbecco's Modified Eagle Medium (DMEM, Cat# C11995500BT) supplemented with 10 % fetal bovine serum. Cells were incubated at 37 °C with 5 % CO_2, and the medium was changed every two days.

The *CRHR1-IT1* sequence was synthesized according to the full-length sequence with an added poly-A tail based on the LINC02210 sequence, NR_026680.3 in NCBI (**Table S4**), and then subcloned into a pcDNA3.1 (+) vector (Genscript, Shanghai, China). OVCAR3 and A2780 cells were seeded in a 24-well plate and incubated at 37 °C for 8 h. Next, the overexpression vector pcDNA3.1 (+)-*CRHR1-IT1* was transfected into OVCAR3 and A2780 cells using Lipofectamine 3000 (Invitrogen, USA) and Opti-MEM (Thermo Fisher Scientific, USA), following the manufacturer's protocol. Transfection conditions of OVCAR-3 included control (0 μg/well vector, null condition), mock (0 μg/well vector, baseline transfection reagents), vehicle (1 μg/well pcDNA3.1(+) vector), and *CRHR1-IT1* overexpression at 0.25, 0.5, and 1 μg/well pcDNA3.1 (+)-*CRHR1-IT1* vector. Transfection conditions of A2780 included control (0 μg/well vector, null condition), mock (0 μg/well vector, baseline transfection reagents), vehicle (1 μg/well pcDNA3.1(+) vector), and *CRHR1-IT1* overexpression at 0.03125, 0.0625, and 0.125 μg/well pcDNA3.1(+)-*CRHR1-IT1* vector. After 6 h of transfection, cells were washed once with 1X PBS, fresh RPMI-1640 or DMEM medium was then added, respectively, and cells were cultured for 48 h post-transfection. RNA samples were collected from control, mock, vehicle, and *CRHR1-IT1* overexpression conditions at the indicated vector concentrations at 24 and 48 h for sequencing. In total, 24 RNA-seq datasets from OVCAR-3 cells were obtained, with two biological replicates per transfection condition.

RNA isolation and quantitative real-time PCR (qRT-PCR)

Cells were lysed, and total RNA was isolated using the PureLink® RNA Mini Kit (Thermo Fisher Scientific, USA) according to the manufacturer's protocol. 1 μg of RNA was used to synthesize cDNA using the PrimeScript™ RT reagent Kit with gDNA Eraser (Takara, Japan). Subsequent qRT-PCR was performed using SuperReal PreMix Plus (SYBR Green) (Tiangen, China). The expression of mRNAs and lncRNAs was normalized to *GAPDH*. Relative gene expression was calculated by the $2^{-\Delta CT}$ method. The primer sequences for *GAPDH*, *CRHR1-IT1*, *CMYC*, *CRHR1*, *FAS*, *JUN*, and *PARP1* are presented in **Table S5**. All qRT-PCR reactions were performed using a CFX96 TOUCH/GelDoc XR + qRT-PCR machine (Bio-Rad, USA), with three technical replicates for each reaction.

Reads processing of collected RNA-seq data from OVCAR-3 cells

RNA was isolated and purified using TRIzol reagent (Invitrogen, Carlsbad, CA, USA). RNA quality was assessed with the Agilent Bioanalyzer 2100 (Agilent, CA, USA), with RIN scores above 7, and confirmed by electrophoresis with denaturing agarose gel. Poly (A) RNA was purified from 1 μg total RNA using Dynabeads Oligo (dT) 25-61005 (Thermo Fisher, CA, USA) through two rounds of

purification. The poly (A) RNA was then fragmented into small pieces using the Magnesium RNA Fragmentation Module (NEB, cat.e6150, USA) at 94 °C for 5–7 min. The cleaved RNA fragments were reverse-transcribed to cDNA using SuperScript™ II Reverse Transcriptase (Invitrogen, cat. 1896649, USA). Strand-specific RNA-seq libraries were prepared using the dUTP method. 2 × 150 bp paried-end sequencing was then performed on the Illumina NovaSeq X Plus. Next, sequence quality was assessed using FastQC (v0.11.9). Adaptors and low-quality bases were trimmed using Trim-galore (v0.6.6). The remaining RNA-seq reads were then aligned to the human genome (hg19/GRCh37) using STAR (v2.7.10a) [80] based on GENCODE v24 annotations [81]. Gene expression levels were quantified using RSEM (v1.3.1) [82].

Weighted gene co-expression network analysis (WGCNA)

Weighted Gene Co-Expression Network Analysis (WGCNA) was performed on 24 RNA-seq data using the R package WGCNA [83]. The top 50 % variablely expressed genes were used. Modules with at least 30 genes were selected. The expression correlation between *CRHR1-IT1* and genes in each module was then estimated. Genes with the absolute value of gene significance (GS) > 0.75 and module membership (MM) >0.75 were defined as key genes for that module.

Functional enrichment analysis and network construction

Functional enrichment analysis was performed using Metascape (https://metascape.org/) with default settings [84]. Network analysis was implemented in ConsensusPathDB (https://cpdb.molgen.mpg.de) [85], which integrates various interaction networks, including binary and complex protein–protein interactions, genetic interactions, metabolic pathways, signaling pathways, gene regulatory networks, drug-target interactions, and biochemical pathways.

Incucyte apoptosis assay for CRHR1-IT1

After 6 h of cell transfection, cells were washed once with 1X PBS and added fresh RPMI-1640 or DMEM medium, respectively. CellEvent™ Caspase-3/7 Green Detection Reagent (Thermo Fisher Scientific, USA) was then added to the cells, which were subsequently incubated in an Incucyte SX5 incubator for 42 h.

Statistical analysis of qRT-PCR and cell apoptosis assays

Statistical analysis of qRT-PCR and cell apoptosis assays was performed using GraphPad Prism 8.0. Data are presented as the mean ± SE, and experiments were repeated at least three times. Two-sided P-values were calculated using unpaired *t*-test analysis for the qRT-PCR assay. For the cell apoptosis assay, two-sided P-values were estimated using one-way ANOVA. Results were considered significant at $^{*}p < 0.05$, $^{**}p < 0.01$, $^{***}p < 0.001$, and $^{****}p < 0.0001$.

Results

Genotype-driven expression changes of PCGs and lncRNAs

To understand the contribution of germline variants to expression changes, we investigated the association between genotype and local expression variations of both PCGs and lncRNAs (Fig. 1A). After stringent quality control **(Materials and methods)**, we selected 348 HGSOC tumor samples (**Table S1**) with matched high-quality genotype and gene expression data to identify PCG-eQTLs. And for lncRNA-eQTL analysis, we adopted quantified expression data of lncRNAs from the same 348 HGSOC tumor samples. We performed eQTL analysis using a linear regression model for PCGs and lncRNAs, respectively, and interrogated SNPs located within a ±1 Mb (*cis*) window of each PCG or lncRNA. The PCG-eQTL analysis identified 7,145 eGenes (that is, genes significantly associated with at least one SNP) at a Storey's *q*-value ≤0.05. Our results successfully replicated the previously identified significant SNP-gene pairs in the ovary from the GTEx with π_1 = 0.99 (where π_1 represents the proportion of true positives) [86], aligning with our own and others' previous identification of genotype-driven expression changes (eQTLs) from the same tissue [39,41,87]. The number of identified eGenes is also in line with previous eQTL study in 44 human tissues from the GTEx Consortium (**Fig. S3**) [86]. For example, we found that the genetic variant rs35478347 had a robust effect (two-sided P-value = 6.0E-06) on *DHX58* expression (Fig. 1B). And the lncRNA-eQTL analysis identified 572 elncRNAs (that is, lncRNAs significantly associated with at least one SNP) (**Table S6**). For instance, we observed that the expression of the lncRNA *LOC284581* (hg19 chr1:205,781,868–205,875,038) was significantly correlated with rs9438393 (two-sided P-value = 3.02E-74) in HGSOC tumor samples (Fig. 1C). Intriguingly, we found that the variance explained by the top associated SNPs decreased dramatically from that for lncRNA expression to protein-coding gene expression and to HGSOC risk (Fig. 1D), suggesting that expression changes of lncRNAs explain a higher portion of HGSOC heritability than PCGs. Moreover, the regulatory significance of the lead SNP on each ePCG or elncRNA increased for SNPs closer to the transcription start site (TSS), suggesting that germline variations in promoter regions have stronger regulatory effects on expression of both PCGs and lncRNAs (Figs. 1E and 1F). In addition, the regulatory effects of germline variants on lncRNAs were generally stronger than on PCGs (Figs. 1E and 1F), consistent with a previous study indicating that lncRNA eQTLs tend to have larger effect sizes than protein-coding eQTLs [56].

Given the substantial genotype-driven expression changes, we next investigated the potential role of germline variants in HGSOC predisposition (Fig. 1G). First, we identified differentially expressed genes (DEGs) in the ovaries of the HGSOC patients (N = 419 from TCGA) and healthy samples (N = 88 from GTEx). We identified 2,689 up-regulated and 4,616 down-regulated genes as DEGs (Fig. 1H), with 76.9 % being protein-coding genes and 19.9 % being lncRNAs (**Fig. S4**). To ascertain the contribution of germline variants in HGSOC predisposition, we overlapped our DEGs and eQTL results. We found that about 6.82 % of the identified DEGs, including 404 PCGs and 94 lncRNAs, could be driven by underlying germline variants (Fig. 1I **and Table S7**). For instance, the eGene *DHX58*, whose expression changes were regulated by germline variant rs35478347 (Fig. 1B), also showed significant differences (two-sided P-value = 1.31E-43) in expression between HGSOC tumors and healthy samples (**Fig. S5**).

In summary, our results suggested that underlying germline variants play important roles in driving expression changes of both PCGs and lncRNAs, which could further contribute to the HGSOC-associated DEGs.

Genotype-driven expression changes are enriched for HGSOC-associated GWAS loci

As the vast majority of GWAS-identified HGSOC risk loci reside in non-coding regions of the genome, these variants might function through regulatory effects on the expression of putative causal PCGs or lncRNAs (Fig. 2A). To understand the underlying biological mechanisms of the observed statistical association between SNPs and HGSOC predisposition, we first overlapped genome-wide significant loci in HGSOC GWAS [33] and in our eQTL signals for both

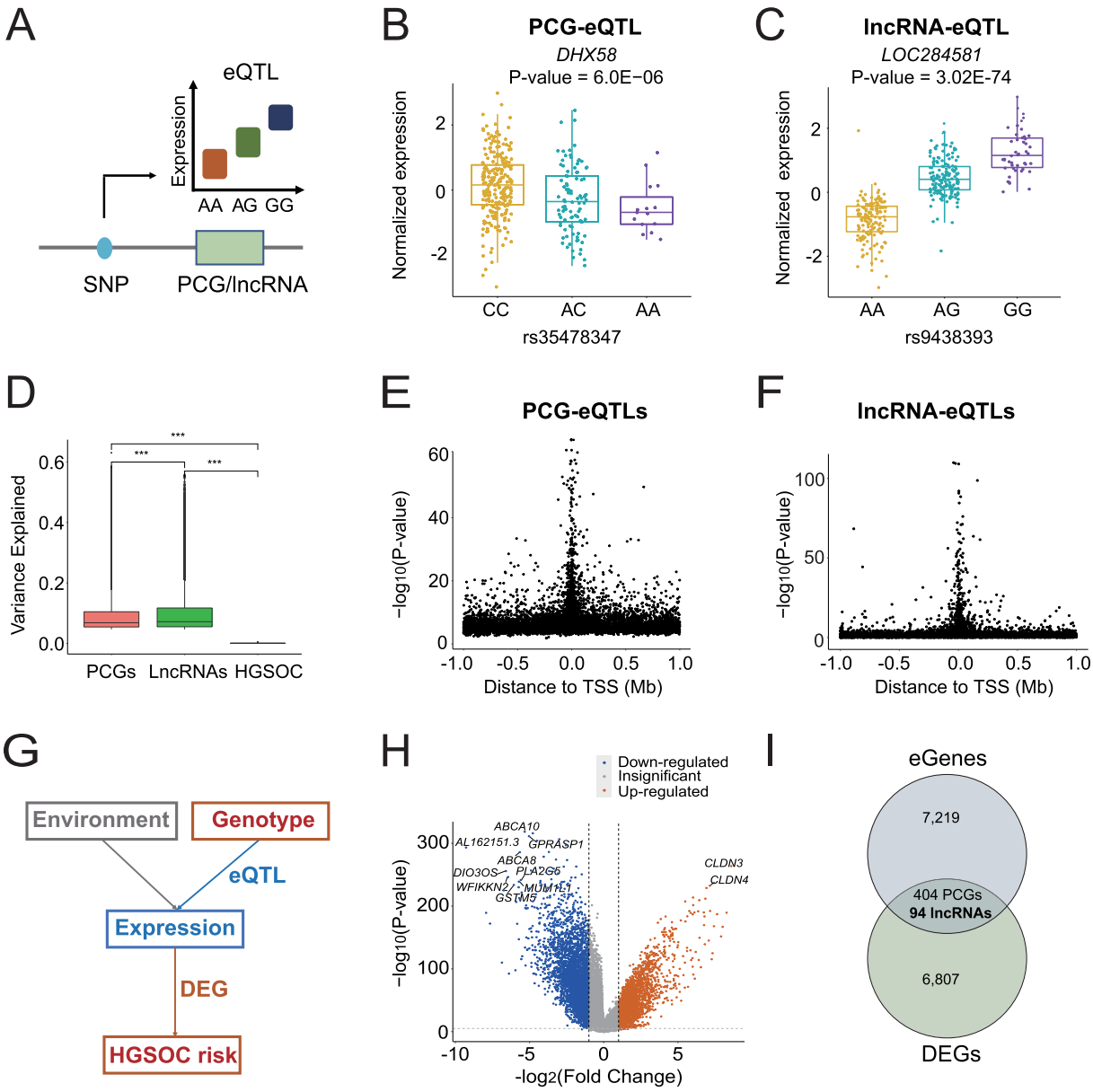

Fig. 1. Genotype-driven expression changes of PCGs and lncRNAs contribute to HGSOC predisposition. (A) Schematic representation of PCG-eQTL and lncRNA-eQTL; genotype-expression association study. Expression changes regulated by a nearby SNP. (B) An example of PCG-eQTL. The genotype of SNP rs35478347 and the gene expression of *DHX58* association in HGSOC tumors (N = 348 samples; two-sided P-value = 6.0E-06). (C) An example of lncRNA-eQTL. The genotype of SNP rs9438393 and the expression of the lncRNA *LOC284581* association in HGSOC tumors (N = 348 samples; two-sided P-value = 3.02E-74). Center lines show the medians; box limits indicate the 25th and 75th percentiles; whiskers extend to the 5th and 95th percentiles. Two-sided P-value was calculated by linear regression model. (D) Distribution of the variance explained in expression of PCGs, lncRNAs, and HGSOC predisposition using the best eSNPs (the lead eQTL). Two-sided P-values were calculated using Student's *t*-test. Statistical significance is indicated by $^{*}p < 0.05$, $^{**}p < 0.01$, $^{***}p < 0.001$, and $^{****}p < 0.0001$. (E) The strength of association (y-axis) of the best eSNPs (the lead eQTL) decreases as the distance (x-axis) from the transcription start site of PCGs increases (N = 348 samples). (F) The strength of association (y-axis) of the best eSNPs (the lead eQTL) decreases as the distance (x-axis) from the transcription start site of lncRNAs increases (N = 348 samples). (G) Both genetic variants and environmental factors contribute to differentially expressed patterns between HGSOC tumor and healthy samples. Genotype-driven expression changes can be uncovered by eQTL analysis, while differentially expressed gene (DEG) identification detects HGSOC-associated genes. (H) Volcano plot. The x-axis is the negative base 2 log of the fold change in gene expression between HGSOC tumor samples (N = 419) and healthy samples (N = 88). The y-axis represents the negative base 10 log of the significance P-value estimated from DEG identification. (I) The number of eGenes influenced by at least one genetic variant, identified by eQTL analysis. DEGs were identified between HGSOC tumor samples (N = 419) and healthy samples (N = 88). Overlapping DEGs, including 404 PCGs and 94 lncRNAs, could be driven by underlying germline variants.

PCGs and lncRNAs, respectively. Genotype-driven expression changes of 51 PCGs and 20 lncRNAs showed associations with HGSOC risk (Fig. 2B). Several putative HGSOC risk genes, such as *HOXB4*, *LERK1*, *MYO19*, *MEIOB*, *MRRF*, *C3orf33*, and *CCDC23*, have been identified as associated with epithelial ovarian cancer in previous independent studies [28,88–93]. Although the top significant GWAS signals were enriched on chromosomes 3, 4, 8, and 9, we observed a strong enrichment of candidate susceptibility genes for HGSOC on chromosome 17 after overlapping with eQTLs. These loci are adjacent to the known EOC and breast cancer marker gene *BRCA1* on chromosome 17. Intriguingly, out of these 51 PCGs, 16 genes (about 31 %) have also been previously implicated as candidate breast cancer susceptibility genes (**Table S8**), including *MAPT* [28,94],*LGALS7* [95],*TBC1D3* [96],*IQCG* [97] and *CCL4* [98] etc. In addition, the elncRNA *ERVK13-1* (Endogenous Retrovirus Group K13 Member 1) has previously been shown an association with

breast cancer [99]. It appears that HGSOC and breast cancer share an extensive expression-based pleiotropy at these loci, consistent with previous observations [28,34].

Next, we performed a Bayesian statistical framework established in colocalization (coloc) analysis [58] to prioritize disease-causing genes, whose genotype-driven expression changes are associated with GWAS signals (Fig. 2C), by integrating HGSOC GWAS with the ovarian tumor eQTL data. Our analysis nominated 10 susceptibility genes for HGSOC, including 6 PCGs and 4 lncRNAs (Fig. 2D **and Table S9**). Consistently, all 6 PCGs, *CHMP4C*, *ARL17A*, *ARL17B*, *LRRC37A*, *LRRC37A2*, and *MAPT*, have been previously identified as HGSOC susceptibility genes using a transcriptome-wide association study (TWAS) [28,100,101]. This cross-method concordance, based on distinct statistical assumptions, strengthens the robustness of our colocalization findings. Notably, around ±100 kb window of SNP rs142045106, we identified one protein-coding gene *MAPT* and 3 lncRNAs, including *CRHR1-IT1*, *KANSL1-AS1*, and *LOC102724391*, as putative disease-causing genes for HGSOC. This suggests a likely functional convergence of *MAPT* and its adjacent lncRNAs at this locus. Emerging studies have reported that *MAPT* expression showed an association with estrogen receptor expression in breast cancer, and an imperfect estrogen-response element has also been identified in the promoter region of *MAPT* [94,102,103]. In addition, the tau protein encoded by *MAPT*, was found almost exclusively bound to microtubules, which plays a pivotal role in mitosis in cancer development as well [104].

Germline variant-regulated transcriptional signals in whole blood and ovarian tumors provide insights into HGSOC biology

HGSOC is often diagnosed at a very late stage and is characterized by an immune-suppressive tumor microenvironment (TME) with limited tumor-infiltrating lymphocytes, rendering it largely refractory to checkpoint inhibitor immunotherapies [105,106]. To explore whether transcriptional changes regulated by germline variants might offer biological insights relevant to HGSOC, we investigated putative disease-causing genes in whole blood by integrating HGSOC GWAS with whole blood eQTL data (from GTEx v7) [70] using Bayesian-test-based colocalization analysis [58]. As illustrated in Fig. 2D, our analysis nominated 12 PCGs and 5 lncRNAs in whole blood. Of these genes, *HOXB2* [28], *HOXB3* [107,108], *PLEKHM1* [109], *RCCD1* [28,34], and *KANSL1* [28,110,111] have been previously implicated as susceptibility genes for epithelial ovarian cancer. Intriguingly, *KANSL1* has been previously identified as an oncogene, whereas the colocalized lncRNA *KANSL1-AS1* showed an opposite trend by assessing the 5-year survival time of 170 HGSOC patients [110]. In addition, the variant rs76640332 within *KANSL1* loci was previously reported to be associated with lymphocyte percentage of leukocytes (two-sided P_{GWAS} = 5E-13) [112].

Next, we evaluated whether these susceptibility genes identified in whole blood could serve as circulating biomarkers for HGSOC. We overlapped the colocalized genes in the ovarian tumor and whole blood (Fig. 2D). *ARL17A*, *LRRC37A2*, and *CRHR1-IT1* were found to show significant differences in expression between HGSOC tumors and healthy samples (Figs. 2E and 2F, **Fig. S6**). We also found that the expression of the overlapping elncRNA *KANSL-AS1* correlated with the EOC marker gene *BRCA2* expression in the TCGA HGSOC tumor samples (Fig. 2G). While these observations do not yet establish diagnostic utility, they suggest that colocalized genes identified in whole blood may represent accessible and promising candidates for future development as less-invasive biomarkers for HGSOC.

Using the genome-scale integrated analysis of gene networks in tissues (GIANT 2.0) [113], we found that the colocalized genes *KANSL1*, *LRRC37A2*, and *ARL17A* were strongly co-expressed in $CD8^+$ T cells and enriched for chromatin organization and regulation of nitrogen compound metabolic process (Fig. 2H **and Table S10**). Nitrogen is one of the essential requirements for *de novo* synthesis of many important nitrogenous compounds, including amino acids and nucleotides, which support the growth of both cancer and immune cells [114]. The competition for available nitrogen between tumor cells and infiltrating $CD8^+$ T cells might further alter the TME [114]. $CD8^+$ T cells are pivotal to the efficacy of cancer immunotherapies [115]. Emerging studies have shown that variations in the fraction of infiltrating $CD8^+$ T cells in the TME can lead to different outcomes in prognosis and treatment response in various malignancies, including breast cancer and HGSOC [116–118].

Single-nucleus resolution transcriptome maps for the human HGSOC tumor

Next, we characterized the expression atlas of PCGs and lncRNAs at single-cell resolution in human HGSOC tumors using snRandom-seq [119,120], a droplet-based, highly sensitive, and full-length single-nuclei RNA-sequencing method optimized for FFPE samples. Because snRandom-seq captures full-length total RNAs with random primers (Fig. 3A), it enables more comprehensive detection of nuclear and long non-coding RNAs than poly(A)-based platforms such as 10x Genomics, thereby providing deeper insights into lncRNA regulation in tumor cells. We manually assigned the clusters to known cell types according to previously reported cell type marker genes [121–124] (Figs. 3B and 3C). Our snRandom-seq analysis characterized the expression patterns of 10,991 PCGs and 1,481 lncRNAs at single-nucleus resolution in 83,188 human HGSOC tumor cells (Figs. 3B and 3C). Given the strong enrichment of candidate susceptibility genes on chromosome 17 (Fig. 2B) by overlapping HGSOC GWAS with tumor eQTLs, we investigated the single-cell expression patterns of these genes. More than 70 % of them showed high expression levels in the immune cells of HGSOC tumors (**Fig. S7**). Intriguingly, this dataset further confirmed the enriched co-expressed network (Fig. 2H) for the colocalized genes *KANSL1*, *LRRC37A2,* and *ARL17A* in T cells of HGSOC tumors (Fig. 3D), with *KANSL1* showing strong T cell expression consistent with its reported association with the lymphocyte percentage of leukocytes [112]. In addition, we also observed that colocalized genes *ARL17A*, *LRRC37A2*, *LRRC37A,* and *KANSL1-AS1*, identified in both HGSOC tumors and whole blood (Fig. 2D), showed prominent expression in immune cells, cancer cells, and proliferative cancer cells. And *MAPT, CHMP4C* and *ARL17B*, identified in HGSOC tumors, were highly expressed in cancer cells and proliferative cancer cells (**Fig. S8**). These observations were largely confirmed in an independent single-cell dataset of human gynecologic tumors from 11 patients generated with 10x Genomics [79] (**Figs. S9-S11**), supporting the robustness of our single-nucleus full-length transcriptome map and its enhanced lncRNA coverage.

The putative roles of CRHR1-IT1 and KANSL1-AS1 in ovarian cancer

Our analysis nominated two putative causal lncRNAs, *CRHR1-IT1* and *KANSL1-AS1*, in chr17q21 for HGSOC (Figs. 2B and 2D). We identified 91 and 65 colocalized signals (with PP4 ranging from 0.80 to 1.00) (**Table S11**) for *CRHR1-IT1* and *KANSL1-AS1*, respectively. 56 of these colocalized signals were observed from the same genomic regions. For instance, centered around the HGSOC GWAS SNP of rs146761208 (two-sided P_{GWAS} = 6.90E-10), colocalized signals were observed for both *CRHR1-IT1* (Fig. 3E) and *KANSL1-AS1* (**Fig. S12**). In this region, the HGSOC-associated GWAS variants were also the causal variants that influence the expression of

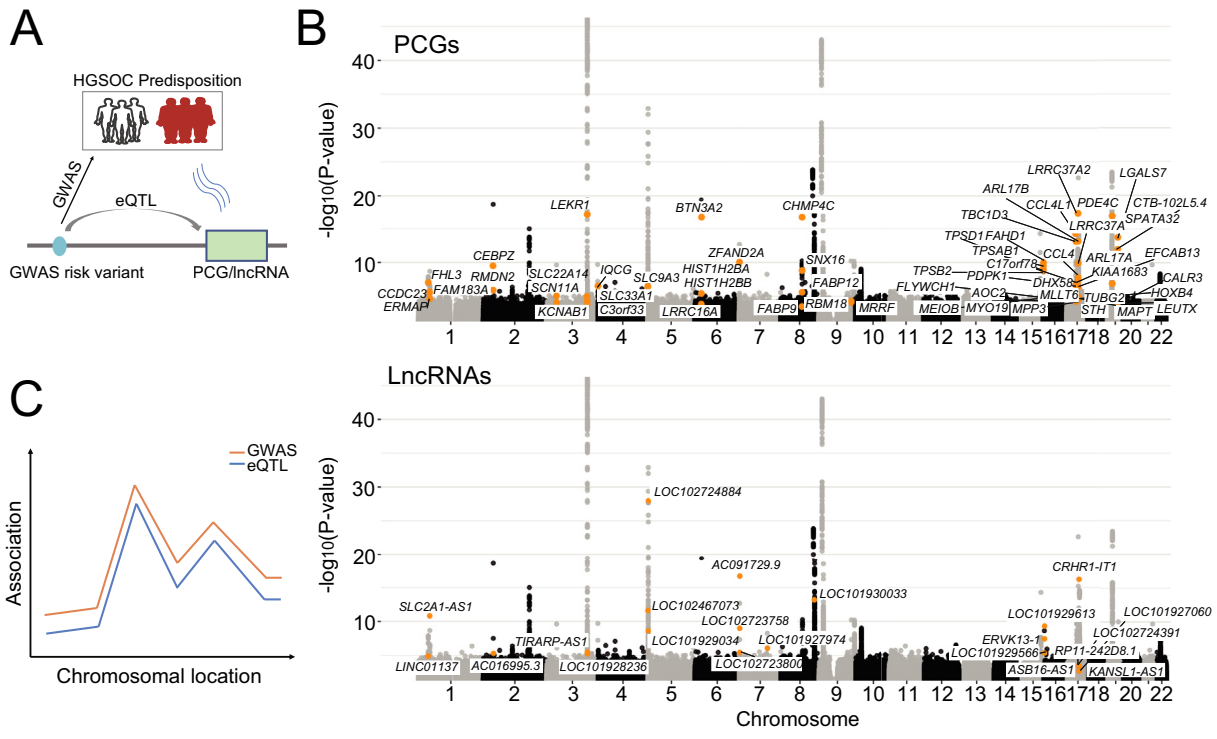
A
HGSOC Predisposition
GWAS
eQTL
GWAS risk variant
PCG/lncRNA
B
PCGs
-log10(P-value)
Chromosome
C
GWAS
eQTL
Association
Chromosomal location
LncRNAs
-log10(P-value)
Chromosome

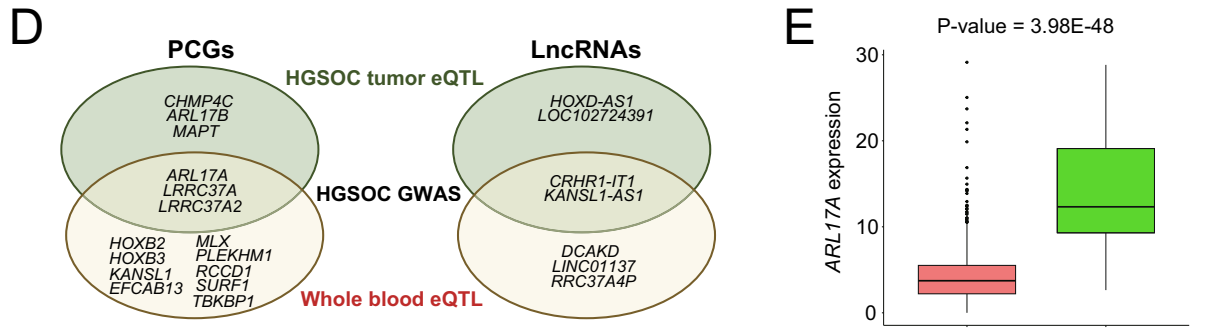
D
PCGs
LncRNAs
HGSOC tumor eQTL
CHMP4C
ARL17B
MAPT
HOXD-AS1
LOC102724391
HGSOC GWAS
ARL17A
LRRC37A
LRRC37A2
CRHR1-IT1
KANSL1-AS1
HOXB2
HOXB3
KANSL1
EFCAB13
MLX
PLEKHM1
RCCD1
SURF1
TBKBP1
DCAKD
LINC01137
RRC37A4P
Whole blood eQTL
E
P-value = 3.98E-48
ARL17A expression
Tumor
N=419
Health
N=88

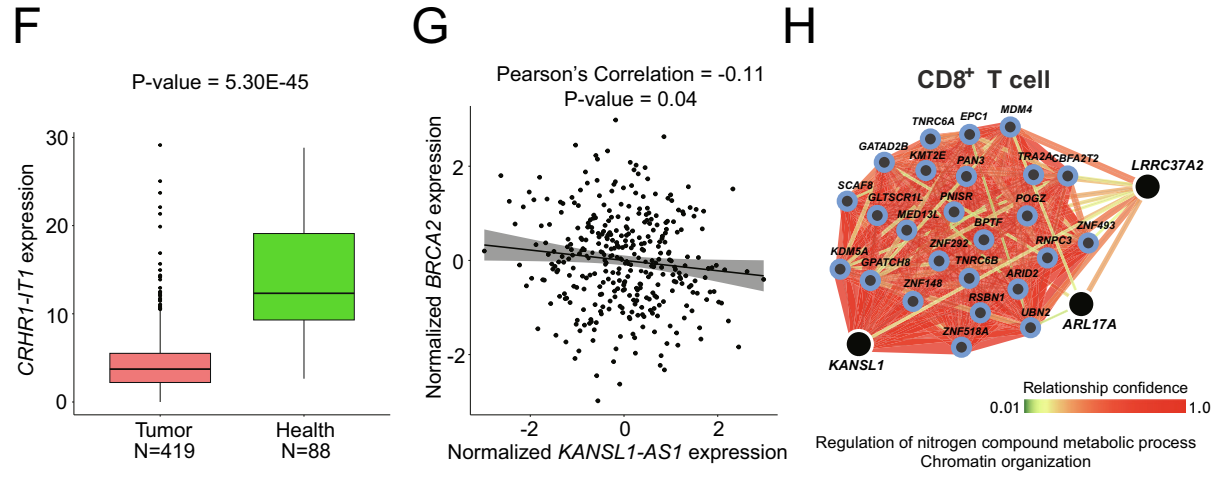
F
P-value = 5.30E-45
CRHR1-IT1 expression
Tumor
N=419
Health
N=88
G
Pearson's Correlation = -0.11
P-value = 0.04
Normalized BRCA2 expression
Normalized KANSL1-AS1 expression
H
CD8+ T cell
LRRC37A2
ARL17A
KANSL1
Relationship confidence
0.01
1.0
Regulation of nitrogen compound metabolic process
Chromatin organization

CRHR1-IT1 and *KANSL1-AS1*. However, our scRNA-seq data of HGSOC tumors showed very low expression of the colocalized lncRNA *CRHR1-IT1*. Combining this with our previous observation shown in Fig. 2F, we hypothesized a potential protective role of *CRHR1-IT1* in HGSOC development.

Functional insights into the lncRNA CRHR1-IT1

To validate the putative roles of *CRHR1-IT1* in HGSOC, we performed quantitative reverse transcription polymerase chain reaction (qRT-PCR) analysis using gradient transfection in the HGSOC cell line OVCAR-3. We explored the biological pathways associated with *CRHR1-IT1* expression changes using RNA-seq data collected from OVCAR-3 cells at 24 and 48 h after transfection. Transfection conditions included: control (0 μg/well vector, null condition), mock (0 μg/well verctor, baseline transfection reagents), vehicle (1 μg/well pcDNA3.1(+) vector), 0.25 (0.25 μg/well pcDNA3.1(+)-*CRHR1-IT1* vector), 0.5 (0.5 μg/well pcDNA3.1(+)-*CRHR1-IT1* vector) and 1 (1 μg/well pcDNA3.1(+)-*CRHR1-IT1* vector) **(Materials and methods)**. We found that transcript expression levels of *CRHR1*, the protein-coding gene corresponding to the lncRNA *CRHR1-IT1* (*CRHR1* intronic transcript 1), were markedly altered after transfection with pcDNA3.1(+)-*CRHR1-IT1* in OVCAR-3 cells **(Fig. S13)**. By performing a weighted gene co-expression network analysis (WGCNA) [83], we identified 9 modules in OVCAR-3 cells and assessed the correlation between the expression of genes within these modules and the lncRNA *CRHR1-IT1* (Figs. 4A and 4B). The 'green' and 'brown' modules exhibited the most significant negative and positive correlations, respectively (Fig. 4B). Of the 357 genes in the 'green' module, 309 were identified as down-regulated in response to *CRHR1-IT1*, whereas 956 of the 1,251 genes in the 'brown' module were up-regulated by *CRHR1-IT1* **(Table S12)**. Functional analysis of these genes indicated enrichment in biological processes regulating cell growth and ovarian function, such as cell cycle, apoptosis, and oocyte meiosis (Fig. 4C). As shown in Fig. 4D, we observed that 309 down-regulated genes exibhited a dramatic decrease in expression at 24 h, while 956 up-regulated genes showed observable increase in expression at 48 h, following transfection with pcDNA3.1(+)-*CRHR1-IT1* in OVCAR-3 cells, compared to the control, mock, and vehicle conditions. Interestingly, the up-regulated genes were likely involved in regulating cell death processes, such as the positive regulation of apoptotic process, whereas the down-regulated genes were enriched in cell cycle processes (Fig. 4E). These findings suggest that *CRHR1-IT1* likely regulates HGSOC cell growth by initially inhibiting cell cycle progression and subsequently promoting apoptosis.

Next, we identified potential transcription factors (TFs) that might regulate *CRHR1-IT1* by combining results from multiple analytical approaches. First, using TRRUST v2 database [125], we found 37 enriched TFs, such as *TP53*, *ATF6*, and *JUN* **(Fig. S14A)**, likely regulators of those 1,265 genes showing *CRHR1-IT1*-associated expression. Second, we prioritized *CRHR1-IT1*-associated genes by assessing gene significance (GS) and module membership (MM) using WGCNA [83]. Our analysis identified 48 key genes from the 'green' and 'brown' modules, which showed the strongest expression association with *CRHR1-IT1* **(Fig. S14B and Table S13)**. Third, we performed a sequence-based interaction prediction for *CRHR1-IT1* using AnnoLnc2 [126], revealing 337 genes that may interact with *CRHR1-IT1* **(Table S14)**. We then evaluated the overlap of predicted TFs for *CRHR1-IT1*, and *JUN* was the only TF present in all three analyses **(Fig. S14C)**. In addition, ChIP-seq data from various cell types confirmed that *JUN* binds to *CRHR1-IT1*, highlighting its potential regulatory role **(Table S15)** [126]. Our RNA-seq data and qRT-PCR results further suggested a strong positive correlation between *CRHR1-IT1* and *JUN* expression (Pearson's correlation = 0.92, two-sided P-value = 1.32E-10; Fig. 4F**, Figs. S15 and S16)**. *JUN*, a crucial transcription factor, which has been previously reported to participate in diverse biological processes including apoptosis [127–133], was also found to be significantly down-regulated in HGSOC samples (Fig. 4G). Subsequent network analysis using the ConsensusPathDB [85] molecular interaction data from 31 public repositories (https://cpdb.molgen.mpg.de) revealed that *JUN* potentially regulate several apoptosis-related genes, such as *ATF3*, *DDIT3*, *TP53, BRCA1,* and *RARG* (Fig. 4H). Notably, *ATF3* has been previously reported to promote apoptosis in cancer cells [134–136]. These findings suggest that *CRHR1-IT1* may co-express with *JUN* to regulate apoptosis in HGSOC cells.

An increase in CRHR1-IT1 expression promotes apoptosis of HGSOC cells

To determine whether *CRHR1-IT1* plays a role in the development of HGSOC cells, we performed a gradient transfection experiment in OVCAR-3 cells. *CRHR1-IT1* expression was significantly increased after transfection with pcDNA3.1(+)-*CRHR1-IT1* in HGSOC cells **(Figs. S13A and S13B)**. Next, we used IncuCyte SX5 and Caspase-3/7 Green Detection Reagent to measure the fluorescence-activated cell intensity in transfected OVCAR3 cells. We observed a dramatic increase in the proportion of apoptotic cells with higher transfection concentrations (Figs. 5A and 5B). And the rate of apoptosis accelerated as the concentration increased at 24 and 48 h after transfection (Figs. 5B-5D). We also found that lncRNA *CRHR1-IT1* slowed down the growth rate of non-apoptotic cells **(Fig. S17)**. Moreover, our qRT-PCR results further confirmed that the expression of genes known to play important roles in apoptosis, including *FAS*, *CMYC*, and *PARP1*, were significantly correlated with lncRNA *CRHR1-IT1* expression (Figs. 5E-5G). These results suggested that elevated *CRHR1-IT1* expression could promote apoptosis in OVCAR-3 cells. To validate

Fig. 2. Integrative analysis of HGSOC GWAS with tumor and blood eQTLs reveals candidate susceptibility genes and regulatory networks. (A) Illustration of the integration analysis of HGSOC GWAS with eQTL data for PCGs and lncRNAs. (B) Miami plots showing overlapped loci that reached genome-wide significance in HGSOC GWAS and in our eQTL data for both PCGs (top) and lncRNAs (bottom), respectively. The orange dots define prioritized PCGs and lncRNAs. The x-axis represents chromosomal location. The y-axis represents the negative base 10 log of the significance P-value. Two-sided P-value was obtained from the HGSOC GWAS study [33]. (C) Illustration of the Bayesian colocalization analysis. This method integrates GWAS and eQTL data to identify loci where the causal variants associated with HGSOC and gene expression are shared (colocalization). (D) We identified 15 protein-coding genes and 7 lncRNAs, where HGSOC predisposition (GWAS) and gene expression (PCG-eQTL/lncRNA-eQTL) share causal genetic variants. Green circles denote colocalized genes identified in HGSOC tumors. Yellow circles denote colocalized genes identified in whole blood. (E) An example of DEG, *ARL17A*, between HGSOC tumor samples (N = 419) and healthy samples (N = 88). Two-sided P-value = 3.98E-48. (F) An example of differientially expressed lncRNA, *CRHR1-IT1*, between HGSOC tumor samples (N = 419) and healthy samples (N = 88). Two-sided P-value = 5.30E-45. Center lines show the medians; box limits indicate the 25th and 75th percentiles; whiskers extend to the 5th and 95th percentiles; outliers are represented by dots. (G) Expression correlation between the lncRNA *KANSL1-AS1* (x-axis) and *BRCA2* (y-axis) in HGSOC tumor samples (N = 348). Two-sided P-value = 0.04. (H) Pathway analysis performed by GIANT 2.0 [113], suggesting that colocalized genes *KANSL1*, *LRRC37A2,* and *ARL17A*, were strongly co-expressed in $CD8^+$ T cells and enriched for chromatin organization and regulation of nitrogen compound metabolic process.

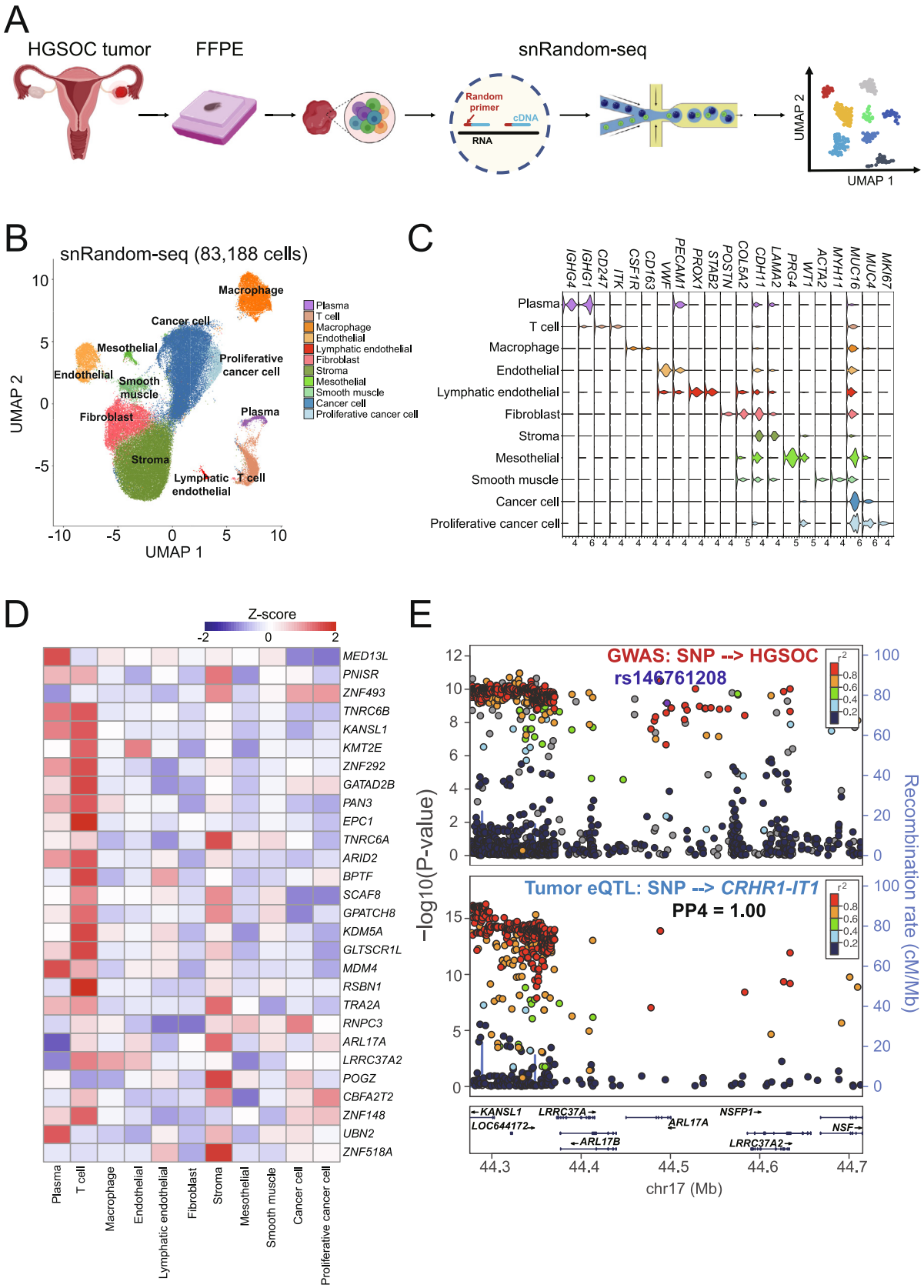

Fig. 3. Single-nucleus resolution transcriptome maps for the human HGSOC tumor. (A) Experimental scheme for snRandom-seq. (B) UMAP plot of single-nucleus transcriptome data from human HGSOC tumors (N = 83,188 cells). Eleven distinct cell clusters were identified using previously reported cell type marker genes [121–124]. (C) Violin plots showing the expression levels of representative marker genes across the 11 cell clusters. (D) Heatmap illustrating the expression patterns of genes involved in the enriched co-expression network for colocalized genes *KANSL1*, *LRRC37A2*, and *ARL17A* in T cells of HGSOC tumors. Mean expression values of the genes were calculated in each cluster. The color scheme represents the Z-score, derived from normalized gene expression levels, indicating relative expression compared to other cell types. (E) LocusZoom plots of HGSOC GWAS variants (top) [33] and HGSOC tumor lnc-eQTLs (bottom) on *CRHR1-IT1*. The x-axis shows the ±200 kb genomic region around rs146761208. The y-axis represents GWAS significance as $-\log_{10}$(two-sided P-value). Each data point represents a variant, with color indicating r^2 (linkage disequilibrium). N = 53,978 individuals for HGSOC GWAS; N = 348 individuals for HGSOC tumor lncRNA-eQTLs.

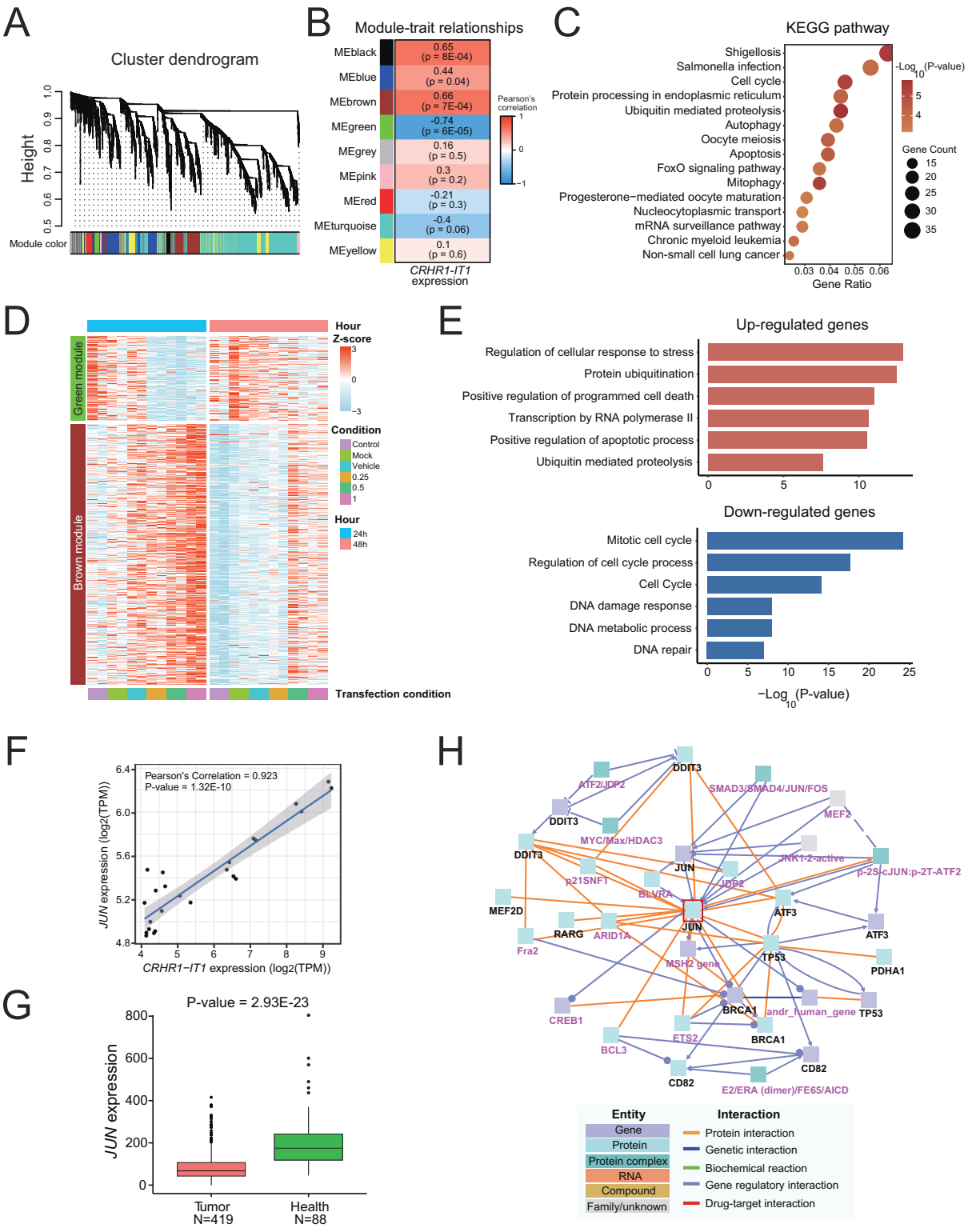

Fig. 4. Co-expression network analysis indicates the potential role of *CRHR1-IT1* in HGSOC development. (A) WGCNA cluster dendrogram and module assignment. Colors in the horizontal bar represent different modules, with genes clustered into 9 distinct modules. (B) Moduel-trait relationships. Pearson's correlation between *CRHR1-IT1* expression and each module is shown. Two-sided P-values represent the significance of these correlations. (C) Functional annotation (KEGG pathway) of genes in the 'green' and 'brown' modules, which exihibited the strongest correlations with *CRHR1-IT1* expression. (D) Expression levels of 956 up-regulated genes and 295 down-regulated genes from the 'green' and 'brown' modules in OVCAR-3 cells. Expression values were calculated from 24 RNA-seq data collected at 24 and 48 h after transfection with vector concentrations of: control (0 μg/well vector, null condition), mock (0 μg/well vector, baseline transfection reagents), vehicle (1 μg/well pcDNA3.1 (+) vector), and increasing concentrations of pcDNA3.1(+)-*CRHR1-IT1* vector: 0.25 μg/well, 0.5 μg/well, and 1 μg/well. (E) Functional annotation of up-regulated genes (top) and down-regulated genes (bottom) in the 'green' and 'brown' modules. (F) Expression correlation between *JUN* and *CRHR1-IT1*. The x-axis represents the $\log_2$ transformed expression of *CRHR1-IT1*, and the y-axis is the $\log_2$ transformed expression of *JUN*. N = 24 samples. (G) An example of DEG, *JUN*, between HGSOC tumor samples (N = 419) and healthy samples (N = 88). Two-sided P-value = 2.93E-23. Center lines show the medians; box limits indicate the 25th and 75th percentiles; whiskers extend to the 5th and 95th percentiles; outliers are represented by dots. (H) Network analysis performed by ConsensusPathDB [85], suggesting that *JUN* potentially regulates several apoptosis-related genes, including *ATF3*, *DDIT3*, *TP53*, *BRCA1*, and *RARG*. Seed nodes are shown in black, and intermediate nodes are shown in purple. 'Andr_human_gene' represents human androgen receptor.

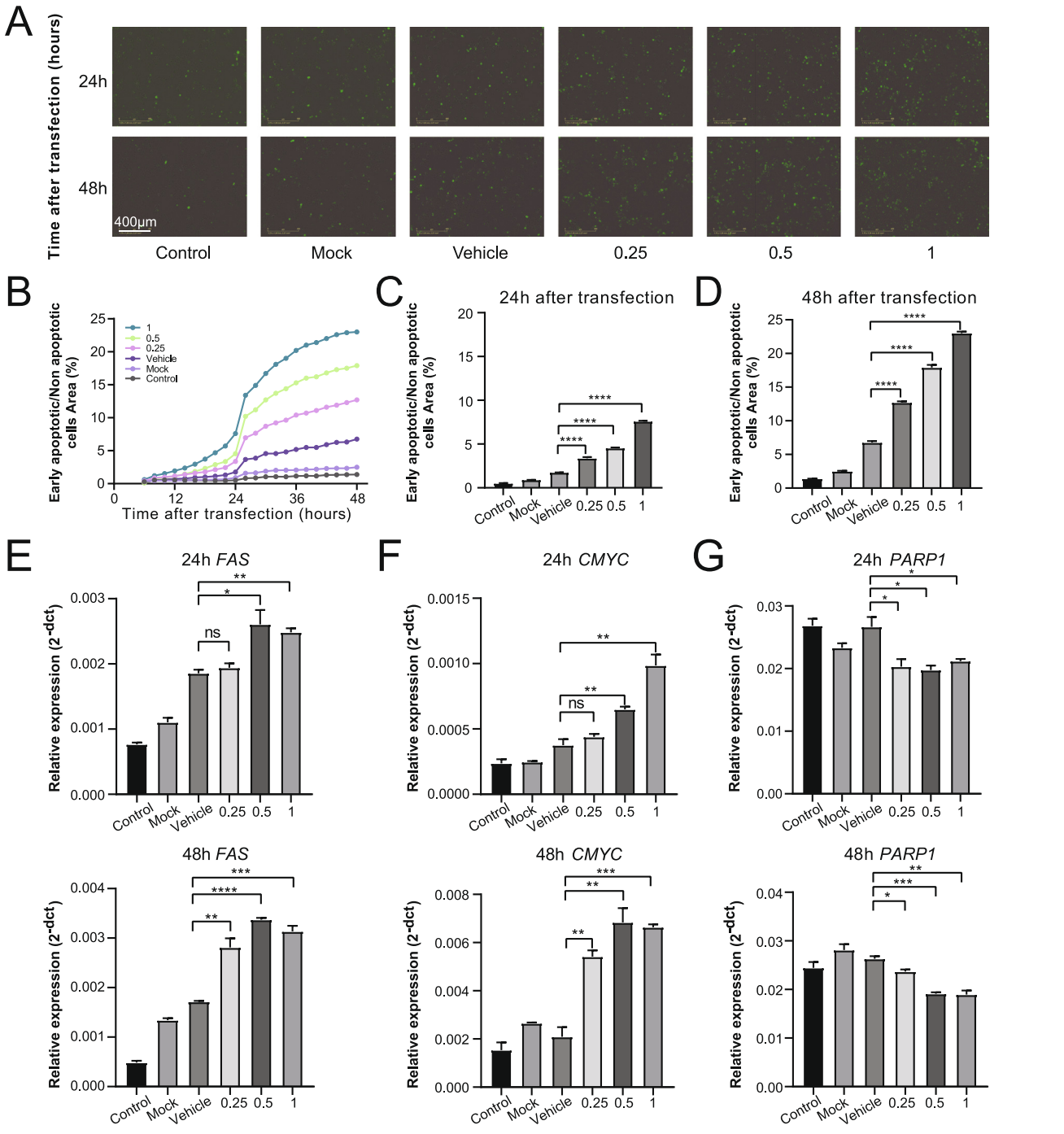

Fig. 5. Increased expression of lncRNA *CRHR1-IT1* promotes apoptosis in OVCAR-3 cells. (A) Representative photographs of cell apoptosis (caspase-3/7 detection reagent displayed as green fluorescence) after transfection with the pcDNA3.1 (+) or pcDNA3.1(+)-*CRHR1-IT1* vectors for 24 or 48 h. Transfection conditions include: control (0 μg/well vector, null condition), mock (0 μg/well vector, baseline transfection reagents), vehicle (1 μg/well pcDNA3.1 (+) vector), and increasing concentrations of pcDNA3.1(+)-*CRHR1-IT1* vector: 0.25 μg/well, 0.5 μg/well, and 1 μg/well. One image per condition is shown out of 48 analyzed images (16imagespertechnicaltriplicate) taken at 10× magnification. (B) Real-time growth monitoring of OVCAR-3 cells was performed using the Incucyte live imaging and analysis system, starting 6 h after transfection. Caspase-3/7 green fluorescence-positive signals represent early apoptotic cells, and negative phase signals represent non-apoptotic cells. Data point is the mean of 3 independent wells per time point ± SE. (C) The ratio of early apoptotic cells to non-apoptotic cells after transfection with the *CRHR1-IT1*_pcDNA3.1(+) vector for 24 h. (D) Ratio of early apoptotic cells to non-apoptotic cells after transfection with the *CRHR1-IT1*_pcDNA3.1(+) vector for 48 h. (E) Expression of *FAS* (24 h, *top*; 48 h, *bottom*) in OVCAR-3 cells at 24 and 48 h after transfection. (F) Expression of *CMYC* (24 h, *top*; 48 h, *bottom*) in OVCAR-3 cells at 24 and 48 h after transfection. (G) Expression of *PARP1* (24 h, *top*; 48 h, *bottom*) in OVCAR-3 cells at 24 and 48 h after transfection. Transfection conditions include: control (0 μg/well vector, null condition), mock (0 μg/well vector, with baseline transfection reagents), vehicle (1 μg/well pcDNA3.1 (+) vector), and increasing concentrations of pcDNA3.1(+)-*CRHR1-IT1* vector: 0.25 μg/well, 0.5 μg/well, and 1 μg/well. Results are shown as mean ± SE of three technical replicates per group. Significance levels are indicated as $^{*}p < 0.05$, $^{**}p < 0.01$, $^{***}p < 0.001$ and $^{****}p < 0.0001$, determined by unpaired *t*-test.

the robustness of these findings, we repeated the gradient transfection and time-course apoptosis assays in another ovarian cancer cell line, A2780, and observed highly consistent results, including dose-dependent apoptosis induction and concordant regulation of apoptosis-related genes (**Figs. S16A, S16B, S18, and S19**). These results together support a conserved pro-apoptotic role of *CRHR1-IT1* in two biologically distinct ovarian cancer cell models.

In summary, our findings highlight the significant role of the lncRNA *CRHR1-IT1* in promoting apoptosis and inhibiting the growth of both OVCAR-3 and A2780 ovarian cancer cells, suggesting that *CRHR1-IT1* could be a promising new therapeutic target for HGSOC.

Discussion

In this study, we defined genotype-driven expression changes for both PCGs (PCG-eQTLs) and lncRNAs (lncRNA-eQTLs). We demonstrated that lncRNAs account for a relatively higher portion of HGSOC heritability compared to PCGs. Our Bayesian-test-based colocalization analysis prioritized 10 HGSOC susceptibility genes, such as *MAPT*, *CHMP4C*, *KANSL1-AS1*, and *CRHR1-IT1*, in HGSOC tumors. We also identified 17 putative causal PCGs and lncRNAs in whole blood, which may provide preliminary clues relevant to early detection and immune-related therapeutic exploration for HGSOC, although these translational implications will require further experimental validation. Using the single-nucleus transcriptome map generated by snRandom-seq in human HGSOC tumors, we further characterized the cell-type-dependent expression patterns of the candidate susceptibility PCGs and lncRNAs. Finally, we focused on the lncRNA *CRHR1-IT1* and demonstrated its crucial role in promoting apoptosis in HGSOC cells.

A central novelty of this work lies in estimating genotype-driven expression variation of HGSOC susceptibility lncRNAs. By defining lncRNA-eQTLs, we directly quantify the regulatory impact of germline variants on lncRNA expression. Our findings suggest that lncRNA expression changes could explain more variation in HGSOC heritability than PCGs. It is noteworthy that a considerable proportion of expression variation associated with HGSOC predisposition appears to be driven by underlying germline variants for both lncRNAs and PCGs. For example, the germline variant rs35478347 influences the expression of *DHX58*, a differentially expressed genes between HGSOC tumors and healthy samples. *DHX58* encodes the RIG-I-like receptor LGP2, which has been previously reported to suppress RIG-I signaling [137] and protect tumor cells from ionizing radiation [138,139]. These findings indicate that it will be critical to integrate genotype-driven expression changes of both lncRNAs and PCGs into future DEG identification to distinguish genetically driven from environmentally driven expression differences.

By integrating HGSOC-associated germline variants (from GWAS) with genotype-driven expression changes of PCGs and lncRNAs, we prioritized putative causal genes for HGSOC. Our initial overlapping results of HGSOC GWAS and eQTL data indicate that approximately 31 % of putative susceptibility genes for HGSOC are shared with breast cancer, including *MAPT*, *LGALS7* and *ERVK13-1*, with strong enrichment on chromosome 17. Using Bayesian-test-based colocalization analysis, we identified 10 susceptibility genes for HGSOC with high fidelity. Notably, all 6 identified PCGs, *CHMP4C*, *ARL17A*, *ARL17B*, *LRRC37A*, *LRRC37A2*, and *MAPT*, showed genotype-driven expression changes associated with HGSOC predisposition in our study, which were independently replicated in a previous study using a different statistical method, TWAS [28,100,101]. TWAS employs distinct modeling assumptions, and this concordance provides additional, methodologically independent support for the robustness of our colocalization findings. We also demonstrate that further investigations of the identified colocalized genes in whole blood may yield new insights that are potentially relevant to early detection or immune-related therapeutic exploration for HGSOC. This is best illustrated by the shared colocalized genes, such as *ARL17A*, *LRRC37A2, KANSL1-AS1,* and *CRHR1-IT1*, whose expression and HGSOC predisposition are not only associated but also share common genetic causal variants in both tumor and whole blood. However, these implications remain preliminary and require extensive mechanistic studies and *in vivo* validation.

The snRandom-seq dataset further supports these findings by providing a more comprehensive view of lncRNA expression at single-nucleus resolution compared with conventional scRNA-seq platforms. Importantly, snRandom-seq also confers a distinct practical advantage: its random-primed reverse transcription strategy enables robust transcriptome profiling from FFPE and partially degraded tissues, allowing recovery of lncRNAs that are typically under-detected in poly(A)-based sc/snRNA-seq platforms. This FFPE compatibility is particularly valuable in HGSOC, where archival FFPE tumor specimens represent a major resource for translational and retrospective studies. These data expand our understanding of the cellular contexts in which susceptibility genes operate.

Our study has several limitations. First, the gene expression data used for eQTL mapping were not explicitly adjusted for tumor purity. However, we incorporated PEER factors [66] to account for hidden confounders, which may partially capture effects of tumor heterogeneity and non-tumor cell contributions. As such, the main conclusions are likely robust, as prioritized colocalized genes show consistent signals across independent datasets and methods, including TWAS. Second, while snRandom-seq provides enhanced sensitivity for non-polyadenylated transcripts and offers single-nucleus resolution, its focus on nuclear RNA limits the detection of cytoplasmic mRNAs relative to whole-cell approaches such as 10x Genomics. Third, although our findings suggest potential early-detection markers and therapeutic avenues, their clinical translation remains hypothetical. Future work may explore circulating lncRNAs as less-invasive biomarkers or RNA-targeted therapies as potential strategies. All these applications will require further mechanistic, *in vivo*, and preclinical studies to validate their feasibility.

Finally, our study highlights multiple lines of converging evidence suggesting a potential pro-apoptotic function of *CRHR1-IT1* in HGSOC cells. Elevated *CRHR1-IT1* expression promoted apoptosis and inhibited the growth of both OVCAR-3 cells and A2780 *in vitro*, demonstrating consistent effects across two biologically distinct ovarian cancer models. These *in vitro* results suggest a possible pro-apoptotic effect of *CRHR1-IT1*, but *in vivo* relevance and clinical significance remain to be established, and additional mechanistic studies will be necessary to fully elucidate the role of *CRHR1-IT1* in HGSOC.

Conclusion

In conclusion, we identified genotype-driven expression changes of both PCGs and lncRNAs in HGSOC tumors. Our study highlights the importance of integrating lncRNA-eQTLs to understand the genetic underpinnings of HGSOC pathogenesis. We report a potential pro-apoptotic role of the lncRNA *CRHR1-IT1 in vitro*, though its *in vivo* and clinical significance remain to be established. These findings also suggest that lncRNAs could represent potential therapeutic avenues or circulating biomarkers, but their translational feasibility requires further mechanistic, *in vivo*, and preclinical investigation.

Consent for publication

Not applicable.

Data availability

Matched genotype and quantified gene expression data for 350 primary HGSOC tumor samples were downloaded from the GDC Data Portal as well (https://www.cancer.gov/ccg/research/genome-sequencing/tcga). The gene expression data in the ovaries of the TCGA HGSOC patients and GTEx healthy samples were downloaded from the UCSC Xena Toil recompute dataset [71] ("TCGA TARGET GTEx" unified RNA-seq cohort) available at https://xenabrowser.net/datapages/?dataset=TcgaTargetGtex_rsem_gene_tpm&host=https://toil.xenahubs.net. The eQTL data for lncRNAs and PCGs are available via a searchable public website https://zenodo.org/records/13760103. RNA sequencing data of OVCAR-3 cells and human HGSOC tumor snRandom-seq data generated in this study are publicly available in the GSA database (https://ngdc.cncb.ac.cn/gsa-human/) under accession numbers HRA009466 [140,141] and HRA008122, respectively.

Ethics approval and consent to participate

Genotype, quantified gene expression data, and clinical records of the 350 HGSOC tumor samples used in this study comply with ethical regulations. Approval and informed consent for collection and sharing were already obtained by the relevant consortia from TCGA. HGSOC tumor specimens for snRandom-seq were obtained from the Biobank of the Zhejiang Cancer Hospital. The sample collection and overall study protocol were reviewed and approved by the Medical Ethics Committee of Zhejiang Cancer Hospital (Approval No.: IRB-2022-728), in accordance with established ethical guidelines for human subjects. All participants had provided written informed consent for biospecimen storage and future research use at the time of surgery; therefore, no additional study-specific consent was required.

Declaration of competing interest

The authors declare that they have no known competing financial interests or personal relationships that could have appeared to influence the work reported in this paper.

Acknowledgements

This work is supported by grants from the National Natural Science Foundation of China [32300534, 32270659 to X.S., 32371537 to Y.K., and 82304907 to G.J.], the Open Project of Jiangsu Provincial Science and Technology Resources (Clinical Resources) Coordination Service Platform [TC2023006 to X.S.], the Key R&D Program of Zhejiang Province [2024SSYS0021 to X.S.], the Fundamental Research Funds for the Central Universities [K20250114 to X.S.], and the hundred talents program of Zhejiang University to X.S.; the Youth Innovation Promotion Association of Chinese Academy of Science [2022098 to J.Z.]; We thank the data resources of HGSOC tumor samples provided by the Cancer Genome Atlas (TCGA, http://cancergenome.nih.gov) managed by the NCI and NHGRI. We thank the technical support from the Core Facilities, Liangzhu Laboratory, Zhejiang University. We thank Dr. Chunjie Jiang and Dr. Fan Wu for assistance in lncRNA characterization. We thank Biorender (© BioRender – biorender.com) for support in schematic representations.

Author contributions

X.S. designed the study and supervised the computational analyses. X.S. and Y.K. designed and supervised the experimental validation in cell lines. X.S. and G.J. designed and supervised the snRandom-seq on HGSOC samples with the help of Y. W. X.S., M. L., D.Z., and C.G. performed computational analyses and manuscript writing. Y.C., Z.Z., H.Z., and S.C. performed the experimental validation of *CRHR1-IT1* in cell lines and manuscript writing with the assistance of F.K.-M. C., X. F., N. K., S. L. and M.L. analyzed data with the help of C.B., Q.Q., C.G., M.J., H.Z., J.W., J. Z., and Z. Z.

Appendix A. Supplementary data

Supplementary data to this article can be found online at https://doi.org/10.1016/j.jare.2026.01.014.

References

[1] Sung H, Ferlay J, Siegel RL, Laversanne M, Soerjomataram I, Jemal A, et al. Global cancer statistics 2020: GLOBOCAN estimates of incidence and mortality worldwide for 36 cancers in 185 countries. CA: Cancer J Clin 2021;71(3):209–49.
[2] Risch HA, Marrett LD, Jain M, Howe GR. Differences in risk factors for epithelial ovarian cancer by histologic type: results of a case-control study. Am J Epidemiol 1996;144(4):363–72.
[3] Pearce CL, Templeman C, Rossing MA, Lee A, Near AM, Webb PM, et al. Association between endometriosis and risk of histological subtypes of ovarian cancer: a pooled analysis of case–control studies. Lancet Oncol 2012;13(4):385–94.
[4] Faber MT, Kjær SK, Dehlendorff C, Chang-Claude J, Andersen KK, Høgdall E, et al. Cigarette smoking and risk of ovarian cancer: a pooled analysis of 21 case–control studies. Cancer Causes Control 2013;24:989–1004.
[5] Alsop K, Fereday S, Meldrum C, DeFazio A, Emmanuel C, George J, et al. BRCA mutation frequency and patterns of treatment response in BRCA mutation–positive women with ovarian cancer: a report from the Australian Ovarian Cancer Study Group. J Clin Oncol 2012;30(21):2654.
[6] Vaughan S, Coward JI, Bast Jr RC, Berchuck A, Berek JS, Brenton JD, et al. Rethinking ovarian cancer: recommendations for improving outcomes. Nat Rev Cancer 2011;11(10):719–25.
[7] Bowtell DD, Böhm S, Ahmed AA, Aspuria P-J, Bast Jr RC, Beral V, et al. Rethinking ovarian cancer II: reducing mortality from high-grade serous ovarian cancer. Nat Rev Cancer 2015;15(11):668–79.
[8] Klotz DM, Wimberger P. Cells of origin of ovarian cancer: ovarian surface epithelium or fallopian tube? Arch Gynecol Obstet 2017;296:1055–62.
[9] Kim J, Park EY, Kim O, Schilder JM, Coffey DM, Cho C-H, et al. Cell origins of high-grade serous ovarian cancer. Cancers 2018;10(11):433.
[10] Prat J. New insights into ovarian cancer pathology. Ann Oncol 2012;23: x111–7.
[11] Peres LC, Cushing-Haugen KL, Köbel M, Harris HR, Berchuck A, Rossing MA, et al. Invasive epithelial ovarian cancer survival by histotype and disease stage. JNCI: J Nat Cancer Inst 2019;111(1):60–8.
[12] Mortlock S, Corona RI, Kho PF, Pharoah P, Seo J-H, Freedman ML, et al. A multi-level investigation of the genetic relationship between endometriosis and ovarian cancer histotypes. Cell Rep Med 2022;3(3).
[13] Liu P, Fu R, Chen K, Zhang L, Wang S, Liang W, et al. ETV5-mediated upregulation of lncRNA CTBP1-DT as a ceRNA facilitates HGSOC progression by regulating miR-188-5p/MAP3K3 axis. Cell Death Dis 2021;12(12):1146.
[14] Ramachandran D, Tyrer JP, Kommoss S, DeFazio A, Riggan MJ, AGBDFSTNHJ, et al. Genome-wide association analyses of ovarian cancer patients undergoing primary debulking surgery identify candidate genes for residual disease. NPJ Genom Med 2024;9(1):19.
[15] Jones MR, Peng P-C, Coetzee SG, Tyrer J, Reyes ALP, Corona RI, et al. Ovarian cancer risk variants are enriched in histotype-specific enhancers and disrupt transcription factor binding sites. Am J Hum Genet 2020;107(4):622–35.
[16] Liu R, Hu R, Zeng Y, Zhang W, Zhou H-H. Tumour immune cell infiltration and survival after platinum-based chemotherapy in high-grade serous ovarian cancer subtypes: a gene expression-based computational study. EBioMedicine 2020;51.
[17] Cuellar-Partida G, Lu Y, Dixon SC, Study AOC, Fasching PA, Hein A, et al. Assessing the genetic architecture of epithelial ovarian cancer histological subtypes. Hum Genet 2016;135:741–56.
[18] Nelson MR, Tipney H, Painter JL, Shen J, Nicoletti P, Shen Y, et al. The support of human genetic evidence for approved drug indications. Nat Genet 2015;47 (8):856–60.
[19] King EA, Davis JW, Degner JF. Are drug targets with genetic support twice as likely to be approved? Revised estimates of the impact of genetic support for drug mechanisms on the probability of drug approval. PLoS Genet 2019;15 (12):e1008489.

[20] Lu Y, Ek WE, Whiteman D, Vaughan TL, Spurdle AB, Easton DF, et al. Most common 'sporadic'cancers have a significant germline genetic component. Hum Mol Genet 2014;23(22):6112–8.
[21] Mucci LA, Hjelmborg JB, Harris JR, Czene K, Havelick DJ, Scheike T, et al. Familial risk and heritability of cancer among twins in Nordic countries. J Am Med Assoc 2016;315(1):68–76.
[22] Hall JM, Lee MK, Newman B, Morrow JE, Anderson LA, Huey B, et al. Linkage of early-onset familial breast cancer to chromosome 17q21. Science 1990;250 (4988):1684–9.
[23] Walsh T, Casadei S, Lee MK, Pennil CC, Nord AS, Thornton AM, et al. Mutations in 12 genes for inherited ovarian, fallopian tube, and peritoneal carcinoma identified by massively parallel sequencing. Proc Natl Acad Sci 2011;108 (44):18032–7.
[24] Loveday C, Turnbull C, Ramsay E, Hughes D, Ruark E, Frankum JR, et al. Germline mutations in RAD51D confer susceptibility to ovarian cancer. Nat Genet 2011;43(9):879–82.
[25] Boyd J, Rubin SC. Hereditary ovarian cancer: molecular genetics and clinical implications. Gynecol Oncol 1997;64(2):196–206.
[26] Narod SA, Madlensky L, Tonin P, Bradley L, Rosen B, Cole D, et al. Hereditary and familial ovarian cancer in southern Ontario. Cancer 1994;74(8):2341–6.
[27] Risch HA, McLaughlin JR, Cole DE, Rosen B, Bradley L, Fan I, et al. Population BRCA1 and BRCA2 mutation frequencies and cancer penetrances: a kin–cohort study in Ontario, Canada. J Natl Cancer Inst 2006;98(23):1694–706.
[28] Gusev A, Lawrenson K, Lin X, Lyra Jr PC, Kar S, Vavra KC, et al. A transcriptome-wide association study of high-grade serous epithelial ovarian cancer identifies new susceptibility genes and splice variants. Nat Genet 2019;51(5):815–23.
[29] Lawrenson K, Kar S, McCue K, Kuchenbaeker K, Michailidou K, Tyrer J, et al. Functional mechanisms underlying pleiotropic risk alleles at the 19p13. 1 breast–ovarian cancer susceptibility locus. Nat Commun 2016;7(1):12675.
[30] Pharoah PD, Tsai Y-Y, Ramus SJ, Phelan CM, Goode EL, Lawrenson K, et al. GWAS meta-analysis and replication identifies three new susceptibility loci for ovarian cancer. Nat Genet 2013;45(4):362–70.
[31] Song H, Ramus SJ, Tyrer J, Bolton KL, Gentry-Maharaj A, Wozniak E, et al. A genome-wide association study identifies a new ovarian cancer susceptibility locus on 9p22. 2. Nat Genet 2009;41(9):996–1000.
[32] Bolton KL, Tyrer J, Song H, Ramus SJ, Notaridou M, Jones C, et al. Common variants at 19p13 are associated with susceptibility to ovarian cancer. Nat Genet 2010;42(10):880–4.
[33] Phelan CM, Kuchenbaecker KB, Tyrer JP, Kar SP, Lawrenson K, Winham SJ, et al. Identification of 12 new susceptibility loci for different histotypes of epithelial ovarian cancer. Nat Genet 2017;49(5):680–91.
[34] Kar SP, Beesley J, Amin Al Olama A, Michailidou K, Tyrer J, Kote-Jarai Z, et al. Genome-wide meta-analyses of breast, ovarian, and prostate cancer association studies identify multiple new susceptibility loci shared by at least two cancer types. Cancer Discov 2016;6(9):1052–67.
[35] Chen K, Ma H, Li L, Zang R, Wang C, Song F, et al. Genome-wide association study identifies new susceptibility loci for epithelial ovarian cancer in Han Chinese women. Nat Commun 2014;5(1):4682.
[36] Kuchenbaecker KB, Ramus SJ, Tyrer J, Lee A, Shen HC, Beesley J, et al. Identification of six new susceptibility loci for invasive epithelial ovarian cancer. Nat Genet 2015;47(2):164–71.
[37] Bojesen SE, Pooley KA, Johnatty SE, Beesley J, Michailidou K, Tyrer JP, et al. Multiple independent variants at the TERT locus are associated with telomere length and risks of breast and ovarian cancer. Nat Genet 2013;45(4):371–84.
[38] Goode EL, Chenevix-Trench G, Song H, Ramus SJ, Notaridou M, Lawrenson K, et al. A genome-wide association study identifies susceptibility loci for ovarian cancer at 2q31 and 8q24. Nat Genet 2010;42(10):874–9.
[39] Sheng X, Guan Y, Ma Z, Wu J, Liu H, Qiu C, et al. Mapping the genetic architecture of human traits to cell types in the kidney identifies mechanisms of disease and potential treatments. Nat Genet 2021;53(9):1322–33.
[40] Qiu C, Huang S, Park J, Park Y, Ko Y-A, Seasock MJ, et al. Renal compartment–specific genetic variation analyses identify new pathways in chronic kidney disease. Nat Med 2018;24(11):1721–31.
[41] Sheng X, Qiu C, Liu H, Gluck C, Hsu JY, He J, et al. Systematic integrated analysis of genetic and epigenetic variation in diabetic kidney disease. Proc Natl Acad Sci 2020;117(46):29013–24.
[42] Lawrenson K, Li Q, Kar S, Seo J-H, Tyrer J, Spindler TJ, et al. Cis-eQTL analysis and functional validation of candidate susceptibility genes for high-grade serous ovarian cancer. Nat Commun 2015;6(1):8234.
[43] Nakamura K, Reid BM, Chen A, Chen Z, Goode EL, Permuth JB, et al. Functional analysis of the 1p34. 3 risk locus implicates GNL2 in high-grade serous ovarian cancer. Am J Hum Genet 2022;109(1):116–35.
[44] White NM, Cabanski CR, Silva-Fisher JM, Dang HX, Govindan R, Maher CA. Transcriptome sequencing reveals altered long intergenic non-coding RNAs in lung cancer. Genome Biol 2014;15:1–16.
[45] Jin X, Ge L-P, Li D-Q, Shao Z-M, Di G-H, Xu X-E, et al. LncRNA TROJAN promotes proliferation and resistance to CDK4/6 inhibitor via CDK2 transcriptional activation in ER+ breast cancer. Mol Cancer 2020;19:1–18.
[46] Liu SJ, Dang HX, Lim DA, Feng FY, Maher CA. Long noncoding RNAs in cancer metastasis. Nat Rev Cancer 2021;21(7):446–60.
[47] Zhang E, He X, Zhang C, Su J, Lu X, Si X, et al. A novel long noncoding RNA HOXC-AS3 mediates tumorigenesis of gastric cancer by binding to YBX1. Genome Biol 2018;19:1–15.
[48] Arun G, Diermeier SD, Spector DL. Therapeutic targeting of long non-coding RNAs in cancer. Trends Mol Med 2018;24(3):257–77.
[49] Fan C, González-Prieto R, Kuipers TB, Vertegaal AC, van Veelen PA, Mei H, et al. The lncRNA LETS1 promotes TGF-β–induced EMT and cancer cell migration by transcriptionally activating a TβR1-stabilizing mechanism. Sci Signal 2023;16(790):eadf1947.
[50] Yong W, Yu D, Jun Z, Yachen D, Weiwei W, Midie X, et al. Long noncoding RNA NEAT1, regulated by LIN28B, promotes cell proliferation and migration through sponging miR-506 in high-grade serous ovarian cancer. Cell Death Dis 2018;9(9):861.
[51] Moradi Marjaneh M, Beesley J, O'Mara TA, Mukhopadhyay P, Koufariotis LT, Kazakoff S, et al. Non-coding RNAs underlie genetic predisposition to breast cancer. Genome Biol 2020;21:1–14.
[52] Yu S, Wang Y, Gong X, Fan Z, Wang Z, Liang Z, et al. LncRNA AGPG confers endocrine resistance in breast cancer by promoting E2F1 activity. Cancer Res 2023;83(19):3220–36.
[53] Xu Q, Deng F, Qin Y, Zhao Z, Wu Z, Xing Z, et al. Long non-coding RNA regulation of epithelial–mesenchymal transition in cancer metastasis. Cell Death Dis 2016;7(6):e2254-e.
[54] Wahlestedt C. Targeting long non-coding RNA to therapeutically upregulate gene expression. Nat Rev Drug Discov 2013;12(6):433–46.
[55] Guo H, Ahmed M, Zhang F, Yao CQ, Li S, Liang Y, et al. Modulation of long noncoding RNAs by risk SNPs underlying genetic predispositions to prostate cancer. Nat Genet 2016;48(10):1142–50.
[56] de Goede OM, Nachun DC, Ferraro NM, Gloudemans MJ, Rao AS, Smail C, et al. Population-scale tissue transcriptomics maps long non-coding RNAs to complex disease. Cell 2021;184(10). pp. 2633–48. e19.
[57] Weinstein JN, Collisson EA, Mills GB, Shaw KR, Ozenberger BA, Ellrott K, et al. The cancer genome atlas pan-cancer analysis project. Nat Genet 2013;45 (10):1113–20.
[58] Giambartolomei C, Vukcevic D, Schadt EE, Franke L, Hingorani AD, Wallace C, et al. Bayesian test for colocalisation between pairs of genetic association studies using summary statistics. PLoS Genet 2014;10(5):e1004383.
[59] Purcell S, Neale B, Todd-Brown K, Thomas L, Ferreira MA, Bender D, et al. PLINK: a tool set for whole-genome association and population-based linkage analyses. Am J Hum Genet 2007;81(3):559–75.
[60] Consortium GP. A global reference for human genetic variation. Nature 2015;526(7571):68.
[61] Yang J, Lee SH, Goddard ME, Visscher PM. GCTA: a tool for genome-wide complex trait analysis. Am J Hum Genet 2011;88(1):76–82.
[62] Delaneau O, Marchini J, Zagury J-F. A linear complexity phasing method for thousands of genomes. Nat Methods 2012;9(2):179.
[63] Howie BN, Donnelly P, Marchini J. A flexible and accurate genotype imputation method for the next generation of genome-wide association studies. PLoS Genet 2009;5(6):e1000529.
[64] Marchini J, Howie B, Myers S, McVean G, Donnelly P. A new multipoint method for genome-wide association studies by imputation of genotypes. Nat Genet 2007;39(7):906.
[65] Harrow J, Frankish A, Gonzalez JM, Tapanari E, Diekhans M, Kokocinski F, et al. GENCODE: the reference human genome annotation for the ENCODE Project. Genome Res 2012;22(9):1760–74.
[66] Stegle O, Parts L, Piipari M, Winn J, Durbin R. Using probabilistic estimation of expression residuals (PEER) to obtain increased power and interpretability of gene expression analyses. Nat Protoc 2012;7(3):500.
[67] Shabalin AA. Matrix eQTL: ultra fast eQTL analysis via large matrix operations. Bioinformatics 2012;28(10):1353–8.
[68] Ongen H, Buil A, Brown AA, Dermitzakis ET, Delaneau O. Fast and efficient QTL mapper for thousands of molecular phenotypes. Bioinformatics 2015;32 (10):1479–85.
[69] Storey JD. A direct approach to false discovery rates. J R Stat Soc Ser B (Stat Methodol) 2002;64(3):479–98.
[70] Consortium G. The Genotype-Tissue Expression (GTEx) pilot analysis: Multitissue gene regulation in humans. Science 2015;348(6235):648–60.
[71] Goldman MJ, Craft B, Hastie M, Repečka K, McDade F, Kamath A, et al. Visualizing and interpreting cancer genomics data via the Xena platform. Nat Biotechnol 2020;38(6):675–8.
[72] Ritchie ME, Phipson B, Wu D, Hu Y, Law CW, Shi W, et al. limma powers differential expression analyses for RNA-sequencing and microarray studies. Nucleic Acids Res 2015;43(7):e47-e.
[73] Consortium G. The GTEx Consortium atlas of genetic regulatory effects across human tissues. Science 2020;369(6509):1318–30.
[74] Le DT, Durham JN, Smith KN, Wang H, Bartlett BR, Aulakh LK, et al. Mismatch repair deficiency predicts response of solid tumors to PD-1 blockade. Science 2017;357(6349):409–13.
[75] Satija R, Farrell JA, Gennert D, Schier AF, Regev A. Spatial reconstruction of single-cell gene expression data. Nat Biotechnol 2015;33(5):495–502.
[76] Stuart T, Butler A, Hoffman P, Hafemeister C, Papalexi E, Mauck WM, et al. Comprehensive integration of single-cell data. Cell 2019;177(7). pp. 1888–902. e21.
[77] Korsunsky I, Millard N, Fan J, Slowikowski K, Zhang F, Wei K, et al. Fast, sensitive and accurate integration of single-cell data with Harmony. Nat Methods 2019;16(12):1289–96.
[78] McInnes L, Healy J, Melville J. Umap: Uniform manifold approximation and projection for dimension reduction. arXiv preprint arXiv:180203426. 2018.

[79] Regner MJ, Wisniewska K, Garcia-Recio S, Thennavan A, Mendez-Giraldez R, Malladi VS, et al. A multi-omic single-cell landscape of human gynecologic malignancies. Mol Cell 2021;81(23):4924–41. e10.
[80] Dobin A, Davis CA, Schlesinger F, Drenkow J, Zaleski C, Jha S, et al. STAR: ultrafast universal RNA-seq aligner. Bioinformatics 2013;29(1):15–21.
[81] Frankish A, Diekhans M, Jungreis I, Lagarde J, Loveland JE, Mudge JM, et al. GENCODE 2021. Nucleic Acids Res 2021;49(D1):D916–23.
[82] Li B, Dewey CN. RSEM: accurate transcript quantification from RNA-Seq data with or without a reference genome. BMC Bioinf 2011;12:1–16.
[83] Langfelder P, Horvath S. WGCNA: an R package for weighted correlation network analysis. BMC Bioinf 2008;9(1):1–13.
[84] Zhou Y, Zhou B, Pache L, Chang M, Khodabakhshi AH, Tanaseichuk O, et al. Metascape provides a biologist-oriented resource for the analysis of systems-level datasets. Nat Commun 2019;10(1):1523.
[85] Kamburov A, Herwig R. ConsensusPathDB 2022: molecular interactions update as a resource for network biology. Nucleic Acids Res 2022;50(D1): D587–95.
[86] Storey JD, Tibshirani R. Statistical significance for genomewide studies. Proc Natl Acad Sci 2003;100(16):9440–5.
[87] Pejman Mohammadi, YoSon Park, Princy Parsana, Segrè Ayellet V, Strober Benjamin J, Zachary Zappala, GCLaAFBAACSEDJRHYJB, P., Simona Volpi, NpmAAGPKSLARLNCMHMRASJ, PSLBMEBPA, NCFNCR. Genetic effects on gene expression across human tissues. Nature 2017;550(7675):204–13.
[88] Qiao S, Hou Y, Rong Q, Han B, Liu P. Tregs are involved in VEGFA/VASH1-related angiogenesis pathway in ovarian cancer. Transl Oncol 2023;32:101665.
[89] Hu F, Yang S, Lv S, Peng Y, Meng L, Gou L, et al. Analysis of AC3-33 gene expression in multiple organ cancer and adjacent normal tissue by RNA in situ hybridization. Oncol Lett 2015;9(6):2795–8.
[90] Juárez-Méndez S, Zentella-Dehesa A, Villegas-Ruíz V, Pérez-González OA, Salcedo M, López-Romero R, et al. Splice variants of zinc finger protein 695 mRNA associated to ovarian cancer. J Ovar Res 2013;6(1):61.
[91] Caburet S, Todeschini A-L, Petrillo C, Martini E, Farran ND, Legois B, et al. A truncating MEIOB mutation responsible for familial primary ovarian insufficiency abolishes its interaction with its partner SPATA22 and their recruitment to DNA double-strand breaks. EBioMedicine 2019;42:524–31.
[92] Song F, Li L, Zhang B, Zhao Y, Zheng H, Yang M, et al. Tumor specific methylome in Chinese high-grade serous ovarian cancer characterized by gene expression profile and tumor genotype. Gynecol Oncol 2020;158 (1):178–87.
[93] Kelly Z, Moller-Levet C, McGrath S, Butler-Manuel S, Kavitha Madhuri T, Kierzek AM, et al. The prognostic significance of specific HOX gene expression patterns in ovarian cancer. Int J Cancer 2016;139(7):1608–17.
[94] Zhang N, Li Y, Sundquist J, Sundquist K, Ji J. Identifying actionable druggable targets for breast cancer: Mendelian randomization and population-based analyses. EBioMedicine 2023:98.
[95] Jones C, Mackay A, Grigoriadis A, Cossu A, Reis-Filho JS, Fulford L, et al. Expression profiling of purified normal human luminal and myoepithelial breast cells: identification of novel prognostic markers for breast cancer. Cancer Res 2004;64(9):3037–45.
[96] Wang B, Zhao H, Zhao L, Zhang Y, Wan Q, Shen Y, et al. Up-regulation of OLR1 expression by TBC1D3 through activation of TNFα/NF-κB pathway promotes the migration of human breast cancer cells. Cancer Lett 2017;408:60–70.
[97] Bjørklund SS, Panda A, Kumar S, Seiler M, Robinson D, Gheeya J, et al. Widespread alternative exon usage in clinically distinct subtypes of invasive ductal carcinoma. Sci Rep 2017;7(1):5568.
[98] Sasaki S, Baba T, Nishimura T, Hayakawa Y, Hashimoto S-i, Gotoh N, et al. Essential roles of the interaction between cancer cell-derived chemokine, CCL4, and intra-bone CCR5-expressing fibroblasts in breast cancer bone metastasis. Cancer Lett 2016;378(1):23–32.
[99] Záveská L, Minářd EJVWL, Slanař MKO. Human endogenous retroviruses in breast cancer: altered expression pattern implicates divergent roles in carcinogenesis. Regulation 2024;14:15.
[100] Head ST, Dezem F, Todor A, Yang J, Plummer J, Gayther S, et al. Cis-and trans-eQTL TWASs of breast and ovarian cancer identify more than 100 susceptibility genes in the BCAC and OCAC consortia. Am J Hum Genet 2024;111(6):1084–99.
[101] Lu Y, Beeghly-Fadiel A, Wu L, Guo X, Li B, Schildkraut JM, et al. A transcriptome-wide association study among 97,898 women to identify candidate susceptibility genes for epithelial ovarian cancer risk. Cancer Res 2018;78(18):5419–30.
[102] Bonneau C, Gurard-Levin ZA, Andre F, Pusztai L, Rouzier R. Predictive and prognostic value of the TauProtein in breast cancer. Anticancer Res 2015;35 (10):5179–84.
[103] Ikeda H, Taira N, Hara F, Fujita T, Yamamoto H, Soh J, et al. The estrogen receptor influences microtubule-associated protein tau (MAPT) expression and the selective estrogen receptor inhibitor fulvestrant downregulates MAPT and increases the sensitivity to taxane in breast cancer cells. Breast Cancer Res 2010;12:1–12.
[104] Papin S, Paganetti P. Emerging evidences for an implication of the neurodegeneration-associated protein tau in cancer. Brain Sci 2020;10 (11):862.
[105] Ozmadenci D, Shankara Narayanan JS, Andrew J, Ojalill M, Barrie AM, Jiang S, et al. Tumor FAK orchestrates immunosuppression in ovarian cancer via the CD155/TIGIT axis. Proc Natl Acad Sci 2022;119(17):e2117065119.
[106] Paracchini L, Mannarino L, Romualdi C, Zadro R, Beltrame L, Fuso Nerini I, et al. Genomic instability analysis in DNA from Papanicolaou test provides proof-of-principle early diagnosis of high-grade serous ovarian cancer. Sci Transl Med 2023;15(725):eadi2556.
[107] Miller KR, Patel JN, Zhang Q, Norris EJ, Symanowski J, Michener C, et al. HOXA4/HOXB3 gene expression signature as a biomarker of recurrence in patients with high-grade serous ovarian cancer following primary cytoreductive surgery and first-line adjuvant chemotherapy. Gynecol Oncol 2018;149(1):155–62.
[108] Coan M, Rampioni Vinciguerra GL, Cesaratto L, Gardenal E, Bianchet R, Dassi E, et al. Exploring the role of fallopian ciliated cells in the pathogenesis of high-grade serous ovarian cancer. Int J Mol Sci 2018;19(9):2512.
[109] Coetzee SG, Shen HC, Hazelett DJ, Lawrenson K, Kuchenbaecker K, Tyrer J, et al. Cell-type-specific enrichment of risk-associated regulatory elements at ovarian cancer susceptibility loci. Hum Mol Genet 2015;24(13):3595–607.
[110] Fejzo MS, Chen H-W, Anderson L, McDermott MS, Karlan B, Konecny GE, et al. Analysis in epithelial ovarian cancer identifies KANSL1 as a biomarker and target gene for immune response and HDAC inhibition. Gynecol Oncol 2021;160(2):539–46.
[111] Yang Y, Chen Y, Xu S, Guo X, Jia G, Ping J, et al. Integrating genome and epigenome data to identify tissue-specific DNA methylation biomarkers for cancer risk. medRxiv 2023;2023(08). pp. 09.23293899.
[112] Astle WJ, Elding H, Jiang T, Allen D, Ruklisa D, Mann AL, et al. The allelic landscape of human blood cell trait variation and links to common complex disease. Cell 2016;167(5). pp. 1415–29. e19.
[113] Wong AK, Krishnan A, Troyanskaya OG. GIANT 2.0: genome-scale integrated analysis of gene networks in tissues. Nucleic Acids Res 2018;46(W1): W65–70.
[114] Kurmi K, Haigis MC. Nitrogen metabolism in cancer and immunity. Trends Cell Biol 2020;30(5):408–24.
[115] Chow A, Perica K, Klebanoff CA, Wolchok JD. Clinical implications of T cell exhaustion for cancer immunotherapy. Nat Rev Clin Oncol 2022;19 (12):775–90.
[116] Zhang L, Conejo-Garcia JR, Katsaros D, Gimotty PA, Massobrio M, Regnani G, et al. Intratumoral T cells, recurrence, and survival in epithelial ovarian cancer. N Engl J Med 2003;348(3):203–13.
[117] Goode E, Block M, Kalli K, Vierkant R, Chen W, Fogarty Z, et al. Ovarian tumor tissue analysis (OTTA) consortium. Dose-response association of CD8+ tumor-infiltrating lymphocytes and survival time in high-grade serous ovarian cancer JAMA. Oncol 2017;3(12):e173290.
[118] Ali HR, Chlon L, Pharoah PD, Markowetz F, Caldas C. Patterns of immune infiltration in breast cancer and their clinical implications: a gene-expression-based retrospective study. PLoS Med 2016;13(12):e1002194.
[119] Xu Z, Zhang T, Chen H, Zhu Y, Lv Y, Zhang S, et al. High-throughput single nucleus total RNA sequencing of formalin-fixed paraffin-embedded tissues by snRandom-seq. Nat Commun 2023;14(1):2734.
[120] Xu Z, Lyu Y, Chen H, Chen Y, Wang Y. Single-nucleus total RNA sequencing of formalin-fixed paraffin-embedded samples using snRandom-seq. Nat Protoc 2025;1–32.
[121] Zheng X, Wang X, Cheng X, Liu Z, Yin Y, Li X, et al. Single-cell analyses implicate ascites in remodeling the ecosystems of primary and metastatic tumors in ovarian cancer. Nature Cancer 2023;4(8):1138–56.
[122] Emont MP, Jacobs C, Essene AL, Pant D, Tenen D, Colleluori G, et al. A single-cell atlas of human and mouse white adipose tissue. Nature 2022;603 (7903):926–33.
[123] Muhl L, Mocci G, Pietilä R, Liu J, He L, Genove G, et al. A single-cell transcriptomic inventory of murine smooth muscle cells. Dev Cell 2022;57 (20). pp. 2426–43. e6.
[124] Chai C, Liang L, Mikkelsen NS, Wang W, Zhao W, Sun C, et al. Single-cell transcriptome analysis of epithelial, immune, and stromal signatures and interactions in human ovarian cancer. Commun Biol 2024;7(1):131.
[125] Han H, Cho J-W, Lee S, Yun A, Kim H, Bae D, et al. TRRUST v2: an expanded reference database of human and mouse transcriptional regulatory interactions. Nucleic Acids Res 2018;46(D1):D380–6.
[126] Ke L, Yang D-C, Wang Y, Ding Y, Gao G. AnnoLnc2: the one-stop portal to systematically annotate novel lncRNAs for human and mouse. Nucleic Acids Res 2020;48(W1):W230–8.
[127] Dhanasekaran DN, Reddy EP. JNK signaling in apoptosis. Oncogene 2008;27 (48):6245–51.
[128] Yang C-W, Lee Y-Z, Hsu H-Y, Wu C-M, Chang H-Y, Chao Y-S, et al. c-Jun-mediated anticancer mechanisms of tylophorine. Carcinogenesis 2013;34 (6):1304–14.
[129] Watabe M, Ito K, Masuda Y, Nakajo S, Nakaya K. Activation of AP-1 is required for bufalin-induced apoptosis in human leukemia U937 cells. Oncogene 1998;16(6):779–87.
[130] Wisdom R, Johnson RS, Moore C. c-Jun regulates cell cycle progression and apoptosis by distinct mechanisms. EMBO J 1999;18(1):188–97.
[131] Xiang D-M, Sun W, Zhou T, Zhang C, Cheng Z, Li S-C, et al. Oncofetal HLF transactivates c-Jun to promote hepatocellular carcinoma development and sorafenib resistance. Gut 2019;68(10):1858–71.
[132] Poindessous-Jazat V, Augery-Bourget Y, Robert-Lezenes J. C-Jun modulates apoptosis but not terminal cell differentiation in murine erythroleukemia cells. Leukemia 2002;16(2):233–43.
[133] Leppä S, Bohmann D. Diverse functions of JNK signaling and c-Jun in stress response and apoptosis. Oncogene 1999;18(45):6158–62.

[134] Yoo KH, Kim D-H, Oh S, Park M-S, Kim H, Ha H-H, et al. Transcriptome analysis upon potassium usnate exposure reveals ATF3-induced apoptosis in human gastric and colon cancer cells. Phytomedicine 2021;91:153655.
[135] Kooti A, Abuei H, Farhadi A, Behzad-Behbahani A, Zarrabi M. Activating transcription factor 3 mediates apoptotic functions through a p53-independent pathway in human papillomavirus 18 infected HeLa cells. Virus Genes 2022;58(2):88–97.
[136] Sato A, Nakama K, Watanabe H, Satake A, Yamamoto A, Omi T, et al. Role of activating transcription factor 3 protein ATF 3 in necrosis and apoptosis induced by 5-fluoro-2′-deoxyuridine. FEBS J 2014;281(7):1892–900.
[137] Rothenfusser S, Goutagny N, DiPerna G, Gong M, Monks BG, Schoenemeyer A, et al. The RNA helicase Lgp2 inhibits TLR-independent sensing of viral replication by retinoic acid-inducible gene-I. J Immunol 2005;175(8):5260–8.
[138] Zheng W, Ranoa DRE, Huang X, Hou Y, Yang K, Poli EC, et al. RIG-I–like receptor LGP2 is required for tumor control by radiotherapy. Cancer Res 2020;80(24):5633–41.
[139] Widau RC, Parekh AD, Ranck MC, Golden DW, Kumar KA, Sood RF, et al. RIG-I–like receptor LGP2 protects tumor cells from ionizing radiation. Proc Natl Acad Sci 2014;111(4):E484–91.
[140] Chen T, Chen X, Zhang S, Zhu J, Tang B, Wang A, et al. The genome sequence archive family: toward explosive data growth and diverse data types. Genomics Proteomics Bioinformatics 2021;19(4):578–83.
[141] Members C-N. Database resources of the national genomics data center, China National Center for Bioinformation in 2022. Nucleic Acids Res 2022;50 (D1):D27.